JCI The Journal of Clinical Investigation

Targeting allograft inflammatory factor-1 reprograms kidney macrophages to enhance repair

Irma Husain, … , Edward B. Thorp, Xunrong Luo

J Clin Invest. 2025. https://doi.org/10.1172/JCI185146.

Research In-Press Preview **Immunology** **Nephrology**

The role of macrophages remains incompletely understood in kidney injury and repair. Their plasticity offers an opportunity to polarize them towards mediating injury resolution in both native and transplanted kidneys undergoing ischemia and/or rejection. Here, we show that infiltrating kidney macrophages augmented their AIF-1 expression after injury. *Aif1* genetic deletion led to macrophage polarization towards a reparative phenotype while halting the development of kidney fibrosis. The enhanced repair was mediated by higher levels of anti-inflammatory and pro-regenerative markers leading to a reduction in cell death and increase in proliferation of kidney tubular epithelial cells following ischemic reperfusion injury. Adoptive transfer of *Aif1*$^{-/-}$ macrophages to *Aif1*$^{+/+}$ mice conferred protection against ischemia reperfusion injury. Conversely, depletion of macrophages reversed the tissue-reparative effects in *Aif1*$^{-/-}$ mice. We further demonstrated an increased expression of AIF-1 in human kidney biopsies from native kidneys with acute kidney injury or chronic kidney disease, as well as in biopsies from kidney allografts undergoing acute or chronic rejection. We conclude that AIF-1 is a macrophage marker of renal inflammation, and its targeting uncouples macrophage reparative functions from profibrotic functions. Thus, therapies inhibiting AIF-1 when ischemic injury is inevitable have the potential to reduce the global burden of kidney disease.

Targeting Allograft Inflammatory Factor-1 reprograms kidney macrophages to enhance repair

Running title: Targeting *Aif1* reprograms macrophages

Irma Husain[1,2], Holly Shah[1], Collin Z. Jordan[1], Naveen R. Natesh[3], Olivia Fay[4], Yanting Chen[5], Jamie Privratsky[5], Hiroki Kitai[1], Tomokazu Souma[1], Shyni Varghese[3,6,7], David N. Howell[4], Edward B. Thorp[8], Xunrong Luo[1,2]

[1]Division of Nephrology, Department of Medicine, Duke University School of Medicine, Durham, North Carolina, USA.

[2]Duke Transplant Center, Duke University School of Medicine, Durham, North Carolina, USA.[3]Department of Biomedical Engineering, Duke University Pratt School of Engineering, Durham, North Carolina, USA

[4]Department of Pathology, Duke University, Durham, North Carolina, USA

[5]Department of Anaesthesiology, Duke University, Durham, North Carolina, USA

[6]Department of Mechanical Engineering and Materials Science, Duke University, Durham, North Carolina, USA

[7]Department of Orthopaedic Surgery, Duke University, Durham, North Carolina, USA

[8]Department of Pathology, Feinberg School of Medicine, Northwestern University, Chicago, Illinois, USA.

***Corresponding author**

Xunrong Luo, M.D., Ph.D.

Division of Nephrology, Department of Medicine

2 Genome CT, MSRBII, Rm 2019, Durham, NC 27710

Phone: (919) 613-1516

Email: xunrong.luo@duke.edu

Disclosure Statement

The authors have declared that no conflict of interest exists

Abstract

The role of macrophages remains incompletely understood in kidney injury and repair. Their plasticity offers an opportunity to polarize them towards mediating injury resolution in both native and transplanted kidneys undergoing ischemia and/or rejection. Here, we show that infiltrating kidney macrophages augmented their AIF-1 expression after injury. *Aif1* genetic deletion led to macrophage polarization towards a reparative phenotype while halting the development of kidney fibrosis. The enhanced repair was mediated by higher levels of anti-inflammatory and pro-regenerative markers leading to a reduction in cell death and increase in proliferation of kidney tubular epithelial cells following ischemic reperfusion injury. Adoptive transfer of *Aif1*$^{-/-}$ macrophages to *Aif1*$^{+/+}$ mice conferred protection against ischemia reperfusion injury. Conversely, depletion of macrophages reversed the tissue-reparative effects in *Aif1*$^{-/-}$ mice. We further demonstrated an increased expression of AIF-1 in human kidney biopsies from native kidneys with acute kidney injury or chronic kidney disease, as well as in biopsies from kidney allografts undergoing acute or chronic rejection. We conclude that AIF-1 is a macrophage marker of renal inflammation, and its targeting uncouples macrophage reparative functions from profibrotic functions. Thus, therapies inhibiting AIF-1 when ischemic injury is inevitable have the potential to reduce the global burden of kidney disease.

Key words: Ischemia-reperfusion injury, pro-reparative macrophage, fibrosis, acute kidney injury, chronic kidney disease, rejection

Introduction

Ischemia followed by reperfusion injury (I/RI) is a common injury to the kidney, and when compounded by maladaptive repair, it results in chronic kidney dysfunction characterized by interstitial fibrosis and tubular atrophy (1, 2). I/RI occurs due to kidney hypoperfusion in a myriad of conditions including septic or cardiogenic shock and major surgeries such as cardiac surgery (3-5). Kidney transplantation is another scenario where the inevitable I/RI leads to delayed graft function and poor long-term outcomes (6, 7). Therefore, I/RI creates a significant global burden of chronic kidney disease (CKD) (8) and negatively affects donor kidney utilization (9). Strategies to restrain I/RI-mediated kidney injury and improve repair would have a wide impact on decreasing the prevalence of CKD and improving the outcomes of transplantation.

It has been demonstrated that macrophages (MΦs) accumulate and persist in the kidney long after the initial I/RI (10, 11), a milieu that promotes macrophage alternative activation. Although these macrophages carry out reparative functions (12-14), they also promote fibrosis (15, 16). Cell-extrinsic factors controlling macrophage functional polarization have been extensively studied, but these studies have yielded limited utility for targeted therapeutics (17). In addition, macrophage-intrinsic mechanisms that control their functional polarization are largely unknown.

AIF-1 was originally identified as an Interferon-γ-inducible Ca^{2+}-binding cytosolic protein (18) primarily expressed in macrophages (19, 20) and has since been implicated in several inflammatory diseases including autoimmune encephalitis (21), diabetes (22), rheumatoid arthritis (23) and chronic cardiac and liver allograft rejection (24, 25). However, the specific role it plays in macrophage-mediated inflammation and the therapeutic potential of its targeting remain poorly understood. Here, we demonstrated that kidney I/RI and allograft rejection are characterized by

a significant upregulation of AIF-1 in kidney macrophages. Using genetic and cellular approaches, we showed that inhibiting AIF-1 allows kidney macrophages to acquire pro-reparative functions post-I/RI thereby reducing renal tubular epithelial cell (RTEC) death, promoting RTEC proliferation, and ultimately preventing kidney fibrosis.

Results

Kidney macrophages upregulate AIF-1 following kidney injury

We have previously interrogated the immune cell landscape of macrophage-mediated inflammation in an allogeneic Balb/c to B6 murine kidney transplantation model using single cell RNA-sequencing (scRNA-seq) (26). Using the same data set, we interrogated the expression pattern of *Aif1* in the kidney allograft during rejection in comparison to naïve control kidneys. As shown in Figure 1A, *Aif1* expression was markedly increased in kidneys undergoing rejection. Feature plots localized *Aif1* transcripts largely to macrophage and monocyte subpopulations in rejecting kidneys, while naive kidneys had few macrophages and monocytes with lower *Aif1* transcripts (Figure 1B). As shown in Figure 1C, macrophages from rejecting kidneys expressed the highest level of *Aif1* transcripts (outlined by black rectangles). We next performed immunostaining for AIF-1 on control naïve and rejecting kidneys (Figure 1D). We noted diffuse staining of AIF-1 in the cortex of rejecting kidneys but not in controls. Presence of such a large number of macrophages after renal transplant is a consequence of both I/RI and allo-immunity. In the clinical setting, chronic allograft dysfunction is characterised by diffuse macrophage infiltration and interstitial fibrosis (27, 28). However, murine models are significantly limited in parsing out the individual effects of ischemia and allo-immunity in mediating chronic allograft nephropathy. Therefore, to investigate specifically the role of AIF-1 in kidney ischemia and ensuing fibrosis, we focused our subsequent experiments using a model of I/RI-mediated kidney fibrosis without alloimmunity.

8 to 12-week-old mice underwent unilateral left kidney ischemia for 30 minutes followed by contralateral non-ischemic right kidney nephrectomy ~48 hours prior to planned euthanasia. We intentionally delayed nephrectomy to optimize animal survival while allowing the initial ischemic injury to result in maladaptive repair and fibrosis (29). The 48-hour interval between contralateral nephrectomy and sacrifice also ensured that the terminal serum creatinine reflected only the function of the ischemic kidney.

Using this I/RI model, we first investigated the kinetics of (1) AIF-1 expression in macrophages; and (2) macrophage infiltration in the ischemic kidney. We used flow cytometry to quantify macrophages and their AIF-1 mean fluorescence intensity (MFI) over the course of 28 days post I/RI and using immunofluorescence, we validated the cellular localization of AIF-1. Unsupervised clustering of $CD45^+$ live cells from kidneys of mice after sham or I/RI (day2, day14 and day28) generated 14 different cell clusters (Figure 2A). Of these, four subpopulations were annotated as macrophages (MΦ 1-4, outlined by the dotted line) due to their universal expression of the canonical macrophage markers F4/80 and CD11b (Supplementary Figure 1). A heatmap showing expression patterns of additional markers (CD11c, CD86, MHC II, Ly6G, CD206 and Ly6c) within these macrophage subpopulations is shown in Supplementary Figure 1. We then determined the localization of AIF-1 within immune cells using tSNE plots. We found AIF-1 to be expressed within MΦ 1-4 subsets (Figure 2B, denoted by the black arrow) at all time points post I/RI as well as in kidneys from sham-operated mice. However, the expression at day28 after I/RI was more pronounced than sham or other earlier time points after I/RI. Of note, the most robust expression was seen in subpopulations MΦ-3 and MΦ-4, both of which also expressed a high level of MHC II, while MΦ-4 expressed the highest levels of CD86 (Supplementary Figure 1). For subsequent quantification of AIF-1 levels by MFI and total macrophage counts, kidney macrophages were gated as $CD45^+Ly6G^-CD11b^+Ly6C^-F4/80^+$ cells (Figure 2C). Total macrophage AIF-1 MFI at day28 post I/RI was significantly higher in comparison to sham or other earlier time points after I/RI. A trend towards increased expression was also observed at day14

but not at day2 post I/RI. Interestingly, macrophage infiltration appeared to persist long after the original ischemic insult in this model. Initially, there was a slight decline in total macrophage numbers at day2 post-I/RI, likely due to ischemic injury and death of resident macrophages themselves. However, at day14, there was a significant increase (~3-fold) in the number of macrophages in the kidney, likely from circulation, and this elevation persisted to day28 post-I/RI. These findings were further confirmed with immunofluorescence staining showing co-expression of AIF-1 with F4/80 in the kidney both in sham-operated and I/RI mice (Figure 2D, "MERGE"). As expected, all kidneys from mice 28 days post I/RI showed marked fibrosis and atrophy (as described in below section). However, AIF-1^{+}F4/80^{+} macrophages appeared to be diffusely distributed throughout the kidney cortex and did not co-localize with specific areas of fibrosis or atrophy. In conclusion, robust and persistent AIF-1 expression is induced in ischemic injury-associated kidney macrophages.

Aif1 deletion protects the kidney from interstitial fibrosis and tubular atrophy (IFTA) post-I/RI

Noting the strong association of AIF-1 with persistent macrophage infiltration following I/RI, we next examined the effects of *Aif1* deletion on the development of kidney fibrosis and atrophy following I/RI. Both *Aif1*$^{+/+}$ (WT) and *Aif1*$^{-/-}$ (KO) mice underwent I/RI followed by interval nephrectomy as described above. We first measured the expression of collagen type III alpha 1 chain gene (*Col3a1*) as it has been associated with multiple fibrotic diseases including kidney fibrosis (30). As shown in Figure 3A, at day28 post I/RI, kidneys from KO mice expressed significantly lower *Col3a1* mRNA in comparison to those from WT mice, while no difference was observed in *Col3a1* expression on day14 post-I/RI (Figure 3A) or at baseline (Supplementary Figure 2A). Furthermore, in WT mice, *Col3a1* expression increased between day14 and day28 post I/RI, suggesting continued progression of fibrosis with time in WT mice. However, in KO mice, there was no further increase of *Col3a1* expression between day14 and day28 post I/RI,

suggesting that progression of fibrosis was halted in KO mice. We next examined the development of kidney interstitial fibrosis (IF) by (1) sirius red staining; and (2) staining of fibronectin, another marker of fibrosis in addition to *Col3a1*. As expected, both sirius red and fibronectin staining were minimal in non-ischemic kidneys (Supplementary Figure 2B). Quantification of both sirius red and fibronectin staining demonstrated significantly less fibrosis on day28 post-I/RI in kidneys from KO mice in comparison to those from WT mice (Figure 3B, 3C). We also examined the degree of tubular atrophy (TA) by H&E staining. As shown in Figure 3D, KO mice demonstrated significantly less TA compared to WT mice on day28 post-I/RI. Consistently across all parameters examined, kidney IFTA continued to worsen from day14 to day28 in WT mice; whereas in KO mice, this progression was halted beyond day14 (Figure 3A-3D). Lastly, we measured kidney weight (Figure 3E) and serial serum creatinine (Figure 3F) as overall measurements for nephron mass and kidney function. As shown in Figure 3E, on day28 post-I/RI, KO kidneys maintained similar weight as sham counterparts, whereas WT kidneys weighted significantly lesser than their sham counterparts. Consistently, serum creatinine was also significantly better in KO mice than in WT mice on day28 (Figure 3F). Collectively, these findings indicate that *Aif1* deletion protects kidneys from the development of IFTA and promotes superior kidney function at day28 following I/RI.

It is important to note that the severity of early injury, as reflected by (1) serum creatinine (Supplementary Figure 3A), (2) tubular injury markers (*Ngal* and *Kim-1,* Supplementary Figure 3B), (3) histopathological grading of renal tubular injury (Supplementary Figure 3C), and renal inflammation by (*Il1β, Nos2,* Supplementary Figure 3B*)* and $CD86^{+}$ inflammatory macrophage infiltration (Supplementary Figure 3D) did not differ between WT and KO groups. Therefore, the protective effect from *Aif1* deletion appeared to be a late, rather than an early, effect.

As an important control, we validated that there were no baseline differences in the WT and KO mice in their kidney macrophage expression of anti-inflammatory (*Arg1, Ym1/Chil3, Il10)* and pro-inflammatory (*Il1β, Il6 and Nlrp3)* gene transcripts (Supplementary Figure 4A), as well as

CD206 and CD86 expression in kidney (Supplementary Figure 4B) and splenic (Supplementary Figure 4C) macrophages. Therefore, an injury stimulus such as I/RI is required to enhance macrophage AIF-1 expression and its deleterious effects; but in an uninjured state, we found no effects of *Aif1* deletion on macrophage phenotype.

Aif1$^{-/-}$ macrophages play a dominant role in kidney protection following I/RI

The predominant expression of AIF-1 in kidney MΦs (Figure 2) and the superior functional outcome in *Aif1*$^{-/-}$ mice following I/RI (Figure 3) led us to hypothesize that the lack of AIF-1 in kidney macrophages was the primary mechanism of protection against the development of IFTA after I/RI. To test our hypothesis, we induced I/RI in WT mice, and starting day7, adoptively transferred *Aif1*$^{-/-}$ bone marrow derived MΦs (BMMΦs) at a dose of $2x10^6$ intravenously every three days until their sacrifice on day28 (Figure 4A). Adoptive transfer of *Aif1*$^{+/+}$ BMMΦs was similarly performed as a control. We started adoptive transfer on day7 post-I/RI to not alter early injury and inflammation which were similar in both WT and KO groups (Supplementary Figure 3). Using congenic markers (CD45.1 for hosts and CD45.2 for adoptively transferred BMMΦs), we confirmed the presence of CD45.2$^+$ macrophages in the kidney, but noted that the number of host CD45.1$^+$ macrophages predominated over that of the transferred CD45.2$^+$ macrophages (Supplementary Figure 5A-5C). On day28 post-I/RI, kidneys from mice receiving *Aif1*$^{-/-}$ BMMΦs showed significantly lesser *Col3a1* mRNA expression (Figure 4B), sirius red positive area (Figure 4C), fibronectin staining (Figure 4D), and tubular atrophy (Figure 4E) in comparison to kidneys from mice receiving *Aif1*$^{+/+}$ BMMΦs. Altogether, these findings translated to a trend in higher kidney weight on day28 in mice receiving *Aif1*$^{-/-}$ BMMΦs (Figure 4F). However, no notable difference of serum creatinine was observed (Supplementary Figure 6). Given the predominance of recipient macrophages (Supplementary Figure 5), it is conceivable that lack of creatinine change at day 28 could reflect the few transferred macrophages relative to the host macrophages in addition to the insensitivity of creatinine in mice as an accurate measurement of small

differences in kidney function (31). Future experiments testing escalating doses of adoptive transferred macrophages may demonstrate further enhancement of kidney function on day 28 post I/RI. These data demonstrate that *Aif1*$^{-/-}$ BMMΦs play a protective role following kidney I/RI in a dominant fashion. Additionally, we also concluded that the significance of targeting AIF-1 predominantly stemmed from infiltrating macrophages from the circulation rather than kidney resident macrophages, since we observed this protective effect with intravenous adoptive transfer of macrophages derived from bone marrow precursors.

Aif1$^{-/-}$ macrophages play an obligatory role in kidney protection following I/RI

To definitively attribute the superior kidney outcome in KO mice post-I/RI to the kidney-infiltrating macrophages, we conducted a macrophage depletion experiment. Here, we depleted macrophages with a course of anti-colony stimulating factor-1R (αCSF1R) in both WT and KO mice after I/RI followed by examination on day28 (Figure 5A). We chose day4 post-I/RI to begin αCSF1R treatment based on the rationale that: (1) depletion prior to I/RI would predominantly remove the kidney resident macrophage subset (32), while in our model the protective effect of KO macrophages appeared likely to be exerted by circulating macrophages; and (2) during the early phase post I/RI, macrophages likely exert a proinflammatory effect[6] in both KO and WT mice. Therefore, we wanted to minimize such a confounder by delaying our depletion.

We first determined the efficacy and specificity of αCSF1R treatment. As shown in Supplementary Figure 7A, in both WT and KO mice treated with αCSF1R (using the schedule in Figure 5A), at day28 post-I/RI, there was a near complete depletion of macrophages in the kidney, whereas other myeloid cells in the kidney (monocytes, neutrophils and dendritic cells) were minimally affected. Macrophage depletion was further confirmed by F4/80 immunofluorescent staining (Supplementary Figure 7B).

We next examined the kidney outcomes of macrophage depletion in WT and KO mice. In WT mice, no significant difference was observed in *Col3a1* mRNA expression (Figure 5B), sirius

red positive area (Figure 5C), fibronectin staining (Figure 5D), tubular atrophy (Figure 5E), kidney weights (Figure 5F) or serum creatinine (Supplementary Figure 8A) between kidneys from mice receiving αCSF1R or control immunoglobulin (CTIg). In contrast, in KO mice, kidneys from mice receiving αCSF1R showed significantly more *Col3a1* mRNA expression (Figure 5G), sirius red positive area (Figure 5H), fibronectin staining (Figure 5I), and tubular atrophy (Figure 5J) on day28 compared to kidneys from CTIg treated mice; and consequently, these kidneys had significantly reduced kidney weights (Figure 5K) and a trend towards a higher serum creatinine (Supplementary Figure 8B) compared to CTIg treated counterparts.

Collectively, these data support that *Aif1*$^{-/-}$ macrophages play an obligatory role in kidney protection following I/RI. Notably, depletion of macrophages in WT mice led to neither a detrimental nor a protective effect following I/RI. This is likely due to the αCSF1R-mediated depletion of heterogeneous and functionally dichotomous populations of macrophages in WT mice (namely, proinflammatory versus reparative; AIF-1 expressing versus non-expressing subsets), resulting in a neutral end result.

Aif1 deletion promotes a reparative phenotype in kidney MΦs in response to I/RI

Based on findings in the above macrophage adoptive transfer (Figure 4) and depletion (Figure 5) experiments, we hypothesized that the superior kidney function post I/RI was largely mediated by the *Aif1* KO macrophages. Before examining *Aif1* KO macrophages in detail, we first determined if *Aif1* deficiency had any effect on non-macrophage immune cell populations post I/RI. As shown in Supplementary Figure 9A-9B and 10, we observed no differences in non-macrophage immune cell populations between WT and KO mice kidneys post I/RI, including non-macrophage myeloid cells (monocytes, neutrophils, dendritic cells) and T cells (CD4 and CD8). Additionally, we did not observe any difference in transcripts of T cell activation, differentiation and effector function post I/RI (Supplementary Figure 9C).

Numerous studies have attempted to define mechanisms of macrophage pro-reparative functions (33-35). These can be broadly categorised into: (1) non-inflammatory clearance of apoptotic cells (efferocytosis); (2) suppression of inflammation; and (3) tissue regeneration. Therefore, we evaluated the expression of molecules associated with these distinct pro-reparative functions in *Aif1*$^{-/-}$ kidney macrophages.

First, we examined CD206, a mannose receptor involved in endocytosis and phagocytosis shown to play an important role in immune homeostasis (36). As shown in Figure 6A, the per cell expression level (MFI) as well as total number of CD206-expressing kidney macrophages were significantly higher in KO mice than in WT mice on day14 post-I/RI. Second, we quantified the relative expression level of Arginase-1(*Arg1*) and Chitinase like-3 (*Chil3*/*Ym1*) transcripts in kidney macrophages (sorted for F4/80^{+} cells) on day14 post I/RI. Arg-1 is a marker of alternatively-activated macrophages shown to promote kidney tubular cell proliferation and repair (37). Chil3/Ym1 has also been associated with alternative macrophage activation, though its precise function is currently unclear (38). As shown in Figure 6B, in kidney macrophages isolated from KO mice, relative expression levels of *Arg1* and *Chil3* were significantly higher than those from WT mice on day14 post-I/RI (all expression levels were normalized to those of sham controls). Interestingly, in WT macrophages where Arg-1 expression was already quite low, we did not find a further correlation of its expression with the level of AIF-1 expression (Supplementary Figure 11).

Next, to assess the effect of these factors, we quantified the burden of tubular cell death *in vivo* by TUNEL staining following I/RI. We utilized background auto-fluorescence to highlight the normal kidney architecture. These TUNEL^{+} nuclei were primarily located in cells surrounding the tubular lumen, therefore likely representing dying renal tubular epithelial cells (RTECs). As shown in Figure 6C, at day14 post-I/RI, the burden of RTEC death (number of TUNEL^{+} cells per high power field (200x)) was comparable between KO and WT kidneys. However, by day28, KO kidneys had significantly fewer TUNEL^{+} cells than WT kidneys. We also examined cell death at

an even earlier time point (day2) post I/RI, and noted a large number of TUNEL$^+$ cells in both WT and KO mice and no difference was observed between the groups (Supplementary Figure 12). From these data, we concluded that the persistence of TUNEL$^+$ cells in kidneys from WT, but not KO, mice on day28 was the result of failed repair in WT mice. To further explore downstream cellular targets of these reparative macrophages, we examined fibroblast activation by measuring alpha smooth muscle actin (*αsma/acta2)* transcripts on day28 post I/RI. We measured this in mice receiving *Aif1*$^{+/+}$ or *Aif1*$^{-/-}$ BMMΦs as in Figure 4. No differences were observed between the two groups (Supplementary Figure 13), which indicated that in our model, *Aif1* deletion did not alter macrophages mediated myofibroblast activation.

Having observed that the absence of *Aif1* augmented polarization of macrophages to a reparative phenotype, we decided next to define the potential regulatory pathways altered by *Aif1* in kidney macrophages *in vivo*. As previously reported in the literature, the presumed time frame of macrophage phenotypic switch after I/RI is between 3-5 days post ischemia (39). Therefore, we examined the gene transcription profile of sorted kidney macrophages on day4 post I/RI using Nanostring nCounter analysis. We performed pathway analysis on differentially expressed genes (DEGs) obtained on comparison of KO macrophages to their WT counterparts post I/RI. We identified that the Wnt/β-catenin signaling pathways were differentially regulated in KO vs WT macrophages (Supplementary Figure 14A). Excessive activation of Wnt signaling has been associated with CKD (40-42) and injured renal tubular cells have been shown to produce Wnt ligands (43, 44). We found that genes that activate the canonical Wnt/β-catenin signaling pathway (*Fzd4* (45), *Ctnnb1* (40), *Cdh1* (46, 47), *Jun* (48, 49)) were downregulated in KO macrophages, whereas genes that inhibit Wnt/β-catenin signaling (*Fzd6* (50), *Sfrp4* (51)) were upregulated in KO macrophages. Additionally, examination of DEGs revealed that KO macrophages expressed higher levels of reparative markers (*Mrc2* (52) and *Retnlb*/*Fizz1* (53), highlighted in orange in Supplementary Figure 14B) in comparison to WT macrophages. Conversely, KO macrophages downregulated genes associated with chronic inflammation and poor healing (*Ly6c1* (54), *Cxcl12*

(55), *Gata2* (56), *Arf6* (57),*Peli1* (58) *Irf1* (59); and *Calr* (60), highlighted in purple in Supplementary Figure 14B) compared to WT macrophages.

Collectively, our unbiased pathway analyses and exploration of the macrophage phenotype suggests that AIF-1/Wnt/β-catenin signaling likely directs the fate of macrophages towards reparative polarization which is characterized by efficient efferocytosis and production of anti-inflammatory humoral factors that together reduces the burden of RTEC death.

Aif1$^{-/-}$ macrophages protect RTECs during hypoxic injury *in vitro*

To directly examine cellular interactions between macrophages and RTECs, we developed an *in vitro* BMMΦ-RTEC co-culture system. As shown in Figure 7A, primary RTECs underwent 18 hours of hypoxia plus simultaneous glucose deprivation (see Methods). At the time of reoxygenation we added transwells carrying either *Aif1*$^{+/+}$ or *Aif1*$^{-/-}$ BMMΦs and glucose-replete media to the culture for an additional 48 hours.

At the end of 48 hours of co-culture, we examined the RTECs for total cell numbers (by DAPI staining) and proliferation (by Ki67 staining). As shown in Figure 7B, following hypoxic injury and reoxygenation, RTECs cultured with *Aif1*$^{-/-}$ BMMΦs exhibited significantly higher total cell numbers as well as a higher number of Ki67-expressing cells in comparison to RTECs cultured alone or with *Aif1*$^{+/+}$ BMMΦs. As a control, we also examined the effect of *Aif1*$^{+/+}$ or *Aif1*$^{-/-}$ BMMΦs on RTECs that did not undergo hypoxia in our co-culture system, and did not observe any differences in RTEC numbers or their proliferation (Supplementary Figure 15).

We next examined the BMMΦ response in the presence of hypoxia-injured RTECs. To enhance cell numbers and replicates for the examination, we cultured *Aif1*$^{+/+}$ or *Aif1*$^{-/-}$ BMMΦs directly in the conditioned media from RTECs undergoing hypoxia and reoxygenation (RTEC-hypoxic-CM) as described above. Interestingly, as shown in Figure 7C, *Aif1*$^{-/-}$ BMMΦs exhibited significantly higher levels of *Arg1* and *Chil3* expression compared to *Aif1*$^{+/+}$ BMMΦs after exposure to RTEC-hypoxic-CM. We also examined the expression of *secreted frizzled protein-4*

(*Sfrp4*), which is an inhibitor of Wnt/β-catenin signaling (61), a pathway that promotes macrophage polarization to a profibrotic phenotype (62). *Aif1*$^{-/-}$ BMMΦs expressed significantly higher levels of *Sfrp4* transcripts in comparison to *Aif1*$^{+/+}$ BMMΦs after treatment with RTEC-hypoxic-CM. No baseline differences were observed when BMMΦs were cultured in media from RTECs that did not undergo hypoxia (data not shown). These *in vitro* findings support our *in vivo* findings in Figure 6B and Supplementary Figure 14.

Taken together, we conclude that *Aif1*$^{-/-}$, but not *Aif1*$^{+/+}$, BMMΦs via inhibition of Wnt signaling, acquire a pro-reparative phenotype when exposed to secreted factors from hypoxia-injured RTECs, and consequently promote RTEC regeneration after injury.

AIF1 is identified in macrophages in injured human kidneys

Having identified in murine models AIF-1 expression patterns in ischemia-provoked acute kidney injury (AKI), fibrosis and atrophy as evidence of CKD development, and in kidney transplant rejection, we next examined human kidneys to determine AIF-1 expression in human kidney immune cells in response to injury. To this end, we generated a human kidney immune cell map by reanalyzing and integrating samples from three publicly available data sets (63-65) of single-nuclear RNA sequencing (sn-RNA seq) data (total of 23 samples; N=8 for healthy controls, N=8 for AKI, and N=7 for CKD) (Supplementary Table 1). We selected the immune cells based on their positive *PTPRC* (encoding CD45) expression. As shown in Figure 8A-B, we observed all the major immune cell types in this integrated map. Macrophage (Mac) and monocyte (Mono) subsets expressed their canonical markers *CD163*, *CD68* and *Fc gamma receptor IIIa (FCGR3A)*. We subsequently generated feature plots for healthy, AKI and CKD groups to visualize *AIF1* transcripts; and quantified the percentage of *AIF1* expressing cells among all "CD163^{+} Mac" and "Mono/Mac" cells in each group (Figure 8C). We found that *AIF1* was primarily expressed in the Mac and Mono subsets, and that its expression was increased in both AKI and CKD relative to healthy controls. We further confirmed this finding with

immunohistochemical staining of AIF-1 and CD68 in 9 human kidney biopsies (n=3 each for healthy controls, AKI and CKD). As shown in Figure 8D, we found that AIF-1 was almost always co-expressed with CD68 in the tubulointerstitial compartment, therefore confirming its predominant expression by kidney macrophages. We further noted a heightened AIF-1 expression in disease states (both AKI and CKD) compared to healthy controls. In addition, we established the relevance of AIF-1 in kidney transplant dysfunction, with AIF-1 and CD68 immunohistochemical staining on transplant kidney biopsies (n=2 for healthy no rejection allografts, n=2 for chronic rejection, and n=3 for acute rejection) (Supplementary Figure 16). In healthy no rejection allografts, we observed scattered $CD68^+$ cells without notable AIF-1 staining through the interstitium, and some CD68 and AIF-1 co-staining within the glomeruli. In contrast, in acute or chronic rejection biopsies, we observed dense infiltration of macrophages ($CD68^+$ cells) with striking AIF-1 staining throughout the cortex, involving both tubulointerstitial and glomerular compartments.

Collectively, these data confirm the association of AIF-1 with injury in both native and transplanted kidneys in humans, and support future investigation of targeting AIF-1 to ameliorate macrophage-mediated kidney injury in humans.

Discussion

In this study, we first demonstrated that two distinct etiologies of kidney injury, kidney transplant rejection and ischemia reperfusion, are both characterized by AIF-1 upregulation in kidney macrophages. For subsequent experiments, we chose to investigate the role of AIF-1 in ischemic injury in the native kidney. We identified that the absence of *Aif1* altered Wnt/β-catenin signaling pathways and induced pro-reparative functions in kidney macrophages. Therefore, *Aif1* deletion protected hosts from progression of kidney injury from I/RI to IFTA. Adoptive transfer of $Aif1^{-/-}$ BMMΦs to WT mice dominantly provided protection against I/RI, whereas depletion of macrophages in KO mice reversed this protection. These results collectively support the

conclusion that AIF-1 plays a critical role in directing the phenotype and function of kidney macrophages following I/RI.

While our findings here were predominantly derived from native kidneys, we believe that they are directly relevant in setting of kidney transplantation. First, AIF-1 expression is enhanced by ongoing allo-immunity, similar to that following I/RI, both in rodents (Figure 1) and in humans (Supplementary Figure 16). Mechanisms for this upregulation and its maintenance are currently unclear, but is likely attributable to a high interferon-ɣ state such as from activated adaptive (Natural Killer, T cells) (66, 67) and innate immune cells (68, 69). The expression kinetics of AIF-1 and it's signaling in kidney allograft macrophages in the longitudinal post-transplant course are currently actively investigated in our lab. Secondly, ischemia is inevitable in kidney transplantation, including that induced by calcineurin inhibitors necessary for chronic immunosuppression. Therefore, much like in the native kidneys, AIF-1 expression is also likely upregulated under these circumstances. As chronic allograft nephropathy (CAN), characterized by kidney fibrosis, is a leading cause of long-term kidney allograft failure, we believe that understanding the role of macrophage AIF-1 in promoting kidney fibrosis may reveal therapeutic targets effective for halting fibrosis and prolonging kidney transplant survival.

Despite utilizing a global *Aif1* knock-out model, we were able to attribute the protective effect of *Aif1* deletion specifically to kidney-infiltrating macrophages from circulation by (1) demonstrating a superior outcome with adoptive transfer of *Aif1*$^{-/-}$ BMMΦs in WT mice following I/RI, and (2) by the reciprocal experiment showing worsening of kidney IFTA with depletion of these protective macrophages in KO mice. Having observed the protective effect with adoptive transfer of *Aif1*$^{-/-}$ BMMΦs derived from bone marrow precursors (Figure 4), we speculate that the inflammatory macrophages with high expression of AIF-1 as described in Figure 2 are of bone marrow origin rather than a kidney resident population. Such an infiltrating population has been previously implicated in chronic inflammation and failed repair (70), and AIF-1 is a potential marker for such inflammation. Definitive determination of the macrophage origin is limited with

our current model. Our future directions include further determining the cell origin in an allogeneic kidney transplant model with congenically labelled cells and testing the protective effect of macrophage *Aif1* deficiency with variable durations of warm and cold ischemia.

Using TUNEL staining, we found similar early tubular cell death in both KO and WT kidneys post I/RI (Supplementary Figure 12); but by day 28, a significantly higher degree of tubular cell death was evident in WT kidneys (Figure 6C). Such continued cell death has been previously described in cases of prolonged ischemia, and is likely a feature of failed repair in AKI to CKD transition (71, 72). This, coupled with our *in vitro* findings that KO macrophages facilitated a reduction in hypoxia-induced RTEC death and increased their proliferation, suggests that ongoing RTEC proliferation in excess of cell death prevents the development of tubular atrophy in kidneys from KO mice. Additionally, the protective effect of *Aif1*$^{-/-}$ BMMΦs on RTECs was exerted in the absence of cell to cell contact (Figure 7). Therefore, we conclude that pro-reparative functions of KO MΦs are mediated by secretory factors and that localization of macrophages to areas of fibrosis or injured tubular cells is likely not necessary for this function. Unlike WT macrophages, the Arginase-1 produced by KO macrophages (Figure 6B, 7C) promotes metabolism of arginine to produce urea and ornithine, which is then converted by ornithine decarboxylase enzyme to polyamines (73). As previously published, these polyamines exert a wide array of anti-inflammatory effects such as reduction of IL-1β and TNF-α (74), as well as repair effects such as angiogenesis (75) and renal tubular cell proliferation (76).

On examining the transcriptional landscape of post I/RI macrophages in the kidney (Supplementary Figure 14), we found that genes associated with Wnt/β-catenin signaling activation were upregulated in macrophages from kidneys in WT but not in KO mice. A diverse array of kidney injury models has shown that the upregulation of renal Wnt/β-catenin pathway and its sustained activation leads to detrimental kidney outcomes (43, 44, 77). Specifically in I/RI, Wnt family of proteins are produced by injured renal tubular cells, and through their binding to cell surface receptors of the Fzd family, they promote signaling via β-catenin (43). Wnt signaling in

macrophages has been shown to control their polarization (78). We found that KO macrophages upregulated genes that inhibit Wnt signaling (e.g. Fzd6, Sfrp4), whereas WT macrophages upregulated genes associated with canonical Wnt signaling activation (e.g. Cdh1, Ctnnb1). Therefore, we conclude that AIF-1 promotes canonical Wnt signaling to promote polarization of macrophages to a profibrotic phenotype. Therefore, AIF-1 has the potential to refine the alternatively activated macrophage phenotype such that it uncouples the reparative from the profibrotic function of these cells.

Aif1 silencing RNA (siRNA) has been previously tested in a murine model of autoimmune diabetes in which a single intraperitoneal injection of *Aif1* siRNA effectively restrained expression of AIF-1 in pancreatic macrophages for 7 days (22). Therefore, *Aif1* siRNA could conceivably be used to mitigate kidney I/RI by promoting the reparative potential of macrophages and preventing AKI to CKD transition. In kidney transplantation, we foresee that targeting AIF-1 can mitigate the adverse effects of kidney ischemia during organ preservation, and ultimately prolong kidney allograft survival.

In summary, we have demonstrated that altering the AIF-1/Wnt/β-catenin pathway enhances kidney macrophage pro-regenerative functions, and ultimately reduces kidney fibrosis and preserves kidney function following I/RI. Therefore, AIF-1 is a promising therapeutic target for the prevention of progression to kidney fibrosis and atrophy where a hemodynamic insult to the kidney is inevitable.

There are potential limitations to our current study. First, it is important to note that αCSF1R depletes all macrophages. As shown in Figure 2A and Supplementary Figure 1, post-injury macrophages are a heterogenous group with varying functions, therefore a more selective depletion strategy could potentially be more definitive. Second, while AIF-1 expression in macrophages was the primary focus of this study, our unsupervised approach as shown in the tSNE plot (Figure 2A) and heatmap (Supplementary Figure 1) also found a small dendritic cell population, annotated as DC-3 due to its expression of CD11c, expressing AIF-1. Additionally,

the expression of AIF-1 has been described in non-immune cells such as podocytes (79), vascular smooth muscle cells (80), and endothelial cells (81). While our depletion and adoptive transfer experiments strongly support that macrophages are the predominant cell population in which AIF-1 manifests its function, future studies utilizing cell-specific *Aif1* deletion will be necessary to elucidate the functional significance of AIF-1 in other cell types.

Methods

Sex as a biological variable

Our study exclusively examined male mice as female sex has been shown to be protective against ischemia-reperfusion injury(82). Further studies would be required to model injury severity using a longer warm ischemic time to induce similar degree of injury as was induced in the male mice in this study with 30 minutes of ischemia. However, we expect the findings to be relevant to female sex as well.

Mice

Aif1$^{-/-}$ C57BL/6J (B6) mice were obtained from Dr. Thorp (Northwestern University) (83). They were subsequently bred and housed at Duke. Male 6 to 10-week-old B6 mice were purchased from the Jackson Laboratory. Mice were age-matched for all experiments. All procedures were approved by Duke IACUC (Protocol# A260-18-11). Each experiment was performed on a cage of animals which served as single experimental unit. 2-3 cages of mice were used per experiment to achieve the desired number of animals per group. For mice that underwent I/RI, sample size was planned assuming 20% attrition due to post procedure related complications. For none to low variability groups such as “sham operated mice”, 3-4 mice per group were considered adequate. For higher variability groups, a larger number of mice (6-8) were used. Sample sizes were not calculated *a priori* based on specific primary outcome. All animals that died prior to the intended date of euthanasia were excluded. No randomization was performed to allocate mice

to control or treatment groups. Confounders were minimized by (1) age matching all mice in each experiment, (2) I/RI performed in alternating sequence between control and treatment groups, (3) using the same pedicle clamps for I/RI across comparison groups, and (4) housing all animals in the same facility.

Warm Kidney Ischemia Reperfusion Injury

Mice (8 to 12-week-old) were given buprenorphine SR for analgesia followed Ketamine/Xylazine for anesthesia. Mice were then shaved and cleaned using betadine. Once the left renal pedicle was exposed, ischemia was induced by placing a pedicle clamp for 30 minutes. Throughout the procedure mice were maintained at 36-37^{o}C on a temperature-controlled heating pad. After surgery, 250µl of saline was administered subcutaneously. For mice that were sacrificed on day14 and day28, contralateral (right) nephrectomy was performed 48hrs prior to assessments. For the day2 time point, right nephrectomy was performed at the same time as the left renal pedicle clamp (day0).

Depletion of Kidney Macrophages

Mice were treated with anti-colony stimulating factor-1R (αCSF1R) antibody (BioXCell, clone AFS98) or control immunoglobulin (CTIg) (BioXCell, Rat IgG2a) by intraperitoneal injections. Treatment was started on day4 post-I/RI. The 1st dose was 50mg/kg followed by 25mg/kg every other day until the day of sacrifice.

Bone Marrow Derived Macrophage (BMMΦ) Generation

Bone marrow cells were obtained from femur and tibia of *Aif1*$^{+/+}$ and *Aif1*$^{-/-}$ mice (6-10-week-old). These cells were grown in culture media with DMEM (Cat# 11320033, Gibco), 10% FBS (Cat# A5256701, Gibco), 1% Pen-Strep (Cat# 15140122, Gibco) and 20ng/ml of M-CSF (Cat# 416-ML, R&D Systems) for 7-10 days before being utilized for experiments.

Adoptive transfer of Aif1$^{-/-}$ BMMΦs

Bone marrow cells from *Aif1*$^{-/-}$ mice were cultured in M-CSF containing media as above. On day 7 or day 10, they were harvested using a cell scraper and resuspended in saline at a concentration of 2x10^4 cells/µl. Mice were injected with 2x10^6 BMMΦs every 3 days intravenously. Treatment was started on day7 post-I/RI and continued until the day of sacrifice.

Adoptive Transfer of CD45.2 BMMΦ to CD45.1 Recipients

B6.SJL-Ptprca Pepcb/BoyJ (CD45.1) mice underwent left kidney I/RI for 30 minutes followed by adoptive transfer of 2x10^6 *Aif1*$^{-/-}$ BMMΦs (CD45.2) starting 7 days post I/RI. In some cases, mice were sacrificed on day 9 post I/RI and the ischemic kidney was evaluated for the presence of CD45.2$^+$ cells and for their F4/80 expression using flow cytometry. B6.SJL-Ptprca Pepcb/BoyJ naïve mice were used as controls for gating strategy.

Renal Tubular Epithelial Cell (RTEC) Hypoxia

RTECs were grown in culture as described above. Glucose- and oxygen-free media was prepared by placing glucose-free DMEM (Gibco Cat#11966025) containing 10% FBS, 10 ng/ml EGF, 1% Penicillin/Streptomycin and 1% Insulin-Transferrin-Selenium in a hypoxia-incubator (O_2 20-30PPM, 37^{o}C) chamber overnight prior to use. On day 7 of RTEC culture, cells were washed and placed in the above overnight-prepared hypoxic-glucose free media in the hypoxia-incubator for 18 hours. This was followed by washing and replacement of the media with glucose-containing media (DMEM/F12, 10% FBS, 1% Penicillin/Streptomycin) and returning to an incubator with environmental levels of oxygen and 5% CO_2 for cocultures with BMMΦs.

RTEC and BMMΦ Coculture

BMMΦs from *Aif1*$^{+/+}$ and *Aif1*$^{-/-}$ mice were cultured in M-CSF containing media in Transwell inserts (0.4 µm pore size, Cat# 07-200-154, Corning) at 1x10^{6} cells per well. M-CSF containing media was washed prior to coculture and replaced with DMEM/F12 containing 10% FBS, and 1% Penicillin/Streptomycin. Once RTECs were retrieved from the hypoxia chamber and washed, transwell inserts with BMMΦs were placed in the wells with RTECs for 48 hours, after which RTECs were washed and fixed with 4% paraformaldehyde prior to staining.

BMMΦ treatment with Hypoxia Conditioned Media

Aif1$^{+/+}$ and *Aif1*$^{-/-}$ BMMΦs were generated as described. RTECs underwent hypoxia followed by re-oxygenation as above. Resulting culture supernatant (conditioned media) was collected after 48hrs of re-oxygenation, centrifuged for 10 minutes at 300g followed by passing through a 0.2µm filter to remove cell debris. 2x10^{6} *Aif1*$^{+/+}$ and *Aif1*$^{-/-}$ BMMΦs were then incubated with 2ml conditioned media in 6-well plates for an additional 48hrs, followed by harvesting in Trizol for RT-qPCR.

Kidney Macrophage Sorting

WT and KO mice were subjected to I/RI or sham surgery. Kidneys were harvested and single-cell suspensions were prepared using mechanical dissociation and collagenase IV digestion. Macrophages were then sorted using EasySep Mouse Biotin Positive Selection Kit II and anti-mouse F4/80 biotin-labelled antibody (StemCell Technologies) per manufacturer's protocol. The enriched cells were more than 90% pure for F4/80^{+} cells as determined by flowcytometry (data not shown).

Nanostring nCounter

Kidney macrophages were sorted from ischemic kidneys on day4 post I/RI as described above. Contralateral non-ischemic kidneys were used as controls. RNA was isolated from sorted MΦs

by QIAGEN RNeasy Micro Kit. 100ng RNA per sample was used for NanoString hybridization. Gene expression was measured using nCounter Mouse Myeloid Innate Immunity V2 Panel. Log2 normalized counts and expression ratios were generated using Rosalind Version 3.38.0.1. Cut off for differentially expressed DEGs was FC <=-1.5 or >=+1.5, and *P* value <0.01. Pathway analysis was performed using WikiPathways, *P* value <0.05 was considered statistically significant.

Kidney Function Assay

Serum from mice post I/RI was collected at sacrifice. 10 µl of serum was shipped to UAB/UCSD O'Brien Center Core C Resource. Serum creatinine was measured via Isotope Dilution LC-MSMS and reported in mg/dl.

Flow Cytometry and Analysis

Animals were euthanized, kidneys were perfused with cold PBS and digested with collagenase IV (2mg/ml for 30 minutes at 37^{o}C). Cells were stained with fluorochrome-conjugated antibodies for 30 minutes at 4^{o}C. After surface staining, cells were fixed, permeabilized (Cytofix/Cytoperm buffers; BD), and stained for intracellular targets at room temperature (RT) for 1 hour. Cells were acquired on a BD Fortessa and analysed using FlowJo (10.8.1, Tree Star LLC). We used the following antibodies: CD45-BUV395(30-F11), CD11b-BUV805(M1/70), CD11c-PE(M1/70), F4/80-FITC(BM8), Ly6C-eFluor450(HK1.6), I-A/I-E-BV786(M5/114.15.2), Ly6G-APC Cy7(RB6-8C5), CD206-BV650(15-2), CD86-Pe-Cy7(GL1(RUO), Arginase 1-PE (A1exF5) (eBioscience, BD Bioscience, Tonbo Biosciences, BioLegend). For AIF-1 intracellular staining, we used purified recombinant anti-Iba1/AIF-1(EPR16588) (Abcam) or isotype rabbit IgG(60024B) (R&D Systems) for 1 hour at RT, followed by anti-rabbit IgG APC-conjugated secondary antibody(F0111) (R&D Systems) for 1 hour at RT. Control staining was performed using kidneys from KO mice. Non-specific staining was blocked using purified anti-mouse CD16/CD32 (2.4G2; Tonbo Biosciences) and goat serum. Dead cells were excluded using Aqua LIVE/DEAD dye (Molecular Probes). We

used FACS to enumerate the absolute count of a specific cell population per kidney using the following formula:

Absolute count of a specific cell population per kidney= {(Total number of a cell type by FACS/total number of events acquired by FACS)}x {(total number of cells by hemocytometer/weight of kidney used) x total kidney weight}

For generation of the tSNE plot, we utilized samples from animals sacrificed on the same day and immunostaining was performed in a single batch to minimize variability. Using the Downsample plugin in FlowJo, we first matched the number of collected events to the same number for each sample, then gated on CD45-expressing live cells. Subsequently, we concatenated the individual samples and generated a tSNE plot using FLOWSOM (84), an R studio plugin for FlowJo, and generated 14 unsupervised cells clusters.

Single-nucleus RNA Sequencing (snRNAseq) Analysis of Human Kidneys

We selected a total of 23 snRNAseq datasets from publicly accessible datasets (Kidney Precision Medicine Project (KPMP) project (https://www.kpmp.org.) (63), GSE195460 (64) and GSE210622 (65) to generate an integrated human kidney immune cell map (N=8, control healthy kidneys; N=8 AKI; and N=7, CKD). We first screened and selected the samples with very low mitochondrial gene expression, an indicator of efficient stripping of cytoplasm during the isolation of nuclei. We then chose datasets to represent both sexes, all AKI stages, and CKD with fibrosis (high interstitial fibrosis and tubular atrophy score) for subsequent analyses (Supplementary Table 1: clinical information). These datasets were further analyzed as we previously performed(85, 86) using an R package Seurat v.4.2.0 for quality control, dimensionality reduction, and cell clustering (87). The snRNAseq matrices were filtered by a custom cut-off (genes expressed in >1 cell, cells expressing more than 500 genes), and cells with %mitochondrial genes < 5% were included. After removing the potential doublets using DoubletFinder (ver. 2.04 (88)), count matrices from each sample were integrated using Harmony, which corrected potential batch effects (89). To

remove any additional confounding source of variation, the mitochondrial mapping percentage was regressed out. A graph-based clustering approach in Seurat was used to cluster the cells in our integrated dataset, and the resolution was set at 1.0. Cluster-defining markers for each cluster were obtained using Seurat's FindAllMarkers command (genes expressed at least in 20% of cells within the cluster, log fold change> 0.25) with the Wilcoxon Rank-Sum test. Based on the marker genes and manual curation of the gene expression pattern of canonical marker genes in UMAP plots, we assigned a cell identity to each cluster. We subsequently selected and re-clustered the *PTPRC* (encoding CD45)-expressing immune cells for assessing the *AIF1* gene expression pattern. This approach yielded 9 cell sub-clusters. Cluster-defining markers for each cluster were again obtained using Seurat's FindAllMarkers command. A cell identity was assigned to each sub-cluster. We then removed cells that contained mixed marker gene expressions or unclassified profiles to yield the final immune cell map with 5,702 nuclei. To calculate the proportion of *AIF1* positive cells we extracted the cells which expressed *AIF1* > 0 (from data slot of SCT assay) and then defined these cells as *AIF1* positive cells and other cells within the monocyte and macrophage cultures were defined as negative cells. We counted the number of positive and negative cells and calculated the percentage of *AIF1* positive macrophages and monocytes.

Statistical Analysis

All data are expressed as mean ± SEM. Statistical analysis was performed using GraphPad Prism 10.01.02 (GraphPad Inc). Normal distribution of the data was assess using a Q-Q plot generated using GraphPad Prism 10.01.02. Data were analysed using two-sided, unpaired, student's t-test when only two groups were compared. When more than two data sets were compared, one-way ANOVA test or two-way ANOVA was performed with adjustment for multiple comparisons using the Tukey test (recommended by Prism). Data is represented as mean ± SEM. *P* value <0.05

was considered significant. The only animals excluded from analysis were those which died prior to date of planned euthanasia.

Study Approval

All animal procedures were approved by Duke IACUC (Protocol# A260-18-11). For human samples, Duke IRB approval (Protocol# Pro00108369) was obtained to request previously collected and archived for-cause biopsies of native and transplant kidneys.

Data Availability Statement

The Nanostring Ncounter data supporting the findings of this study are openly available in the Gene Expression Omnibis (GEO) repository at GSE252904 accession number. The results here are in whole or part based upon data generated by the Kidney Precision Medicine Project. Accessed March 11, 2023. https://www.kpmp.org. For snRNA sequencing of human kidney samples, the following additional GEO repositories were utilized GSE195460 and GSE210622. Values for all data points in graphs are reported in the Supporting Data Values file.

Author contributions

I.H. and X.L. designed the study; I.H., H.S., C.Z.J., and O.F. performed the experiments; Y.C. and J.P. assisted with hypoxia chamber experiments; I.H. and X.L. analysed the data; N.R.N and S.V. performed scRNAseq analyses of murine samples, H.K. and T.S. performed snRNAseq analyses of human samples; D.N.H. provided human biopsy samples, and I.H. and X.L. wrote the manuscript. E.T. and X.L. edited the manuscript.

Acknowledgements

This work was supported by the American Society of Nephrology Ben J Lipps Research Fellowship (IH) and NIH R01HL139812 (XL). We would like to thank the Henry E. Haller Jr.

Foundation for their generous support of this work (XL). In addition, we would like to thank Dr. Robert Fairchild and Ms. Karen Keslar for their assistance with Nanostring data analysis who are supported by UO1 AI063594 for the Clinical Trials in Organ Transplantation (CTOT) NanoString Core.

References

1. Sharfuddin AA, and Molitoris BA. Pathophysiology of ischemic acute kidney injury. *Nature Reviews Nephrology.* 2011;7(4):189-200.
2. Bonventre JV, and Yang L. Cellular pathophysiology of ischemic acute kidney injury. *J Clin Invest.* 2011;121(11):4210-21.
3. Vives M, et al. Cardiac surgery-associated acute kidney injury. *Interact Cardiovasc Thorac Surg.* 2014;18(5):637-45.
4. Hoste EA, et al. The epidemiology of cardiac surgery-associated acute kidney injury. *Int J Artif Organs.* 2008;31(2):158-65.
5. Hoste EA, et al. Epidemiology of acute kidney injury in critically ill patients: the multinational AKI-EPI study. *Intensive Care Med.* 2015;41(8):1411-23.
6. Peters-Sengers H, et al. Impact of Cold Ischemia Time on Outcomes of Deceased Donor Kidney Transplantation: An Analysis of a National Registry. *Transplantation Direct.* 2019;5(5):e448.
7. Hariharan S, et al. Post-transplant renal function in the first year predicts long-term kidney transplant survival. *Kidney Int.* 2002;62(1):311-8.
8. Sykes L, et al. The influence of multiple episodes of acute kidney injury on survival and progression to end stage kidney disease in patients with chronic kidney disease. *PLoS One.* 2019;14(7):e0219828.

9. Yarlagadda SG, et al. Association between delayed graft function and allograft and patient survival: a systematic review and meta-analysis. *Nephrol Dial Transplant.* 2009;24(3):1039-47.
10. Han HI, et al. The role of macrophages during acute kidney injury: destruction and repair. *Pediatric nephrology (Berlin, Germany).* 2019;34(4):561-9.
11. Palmer MB, et al. Quantification and localization of M2 macrophages in human kidneys with acute tubular injury. *International journal of nephrology and renovascular disease.* 2014;7:415-9.
12. Shin NS, et al. Arginase-1 Is Required for Macrophage-Mediated Renal Tubule Regeneration. 2022;33(6):1077-86.
13. Lech M, et al. Macrophage phenotype controls long-term AKI outcomes--kidney regeneration versus atrophy. *Journal of the American Society of Nephrology : JASN.* 2014;25(2):292-304.
14. Ricardo SD, et al. Macrophage diversity in renal injury and repair. *The Journal of Clinical Investigation.* 2008;118(11):3522-30.
15. Lee S, et al. Distinct macrophage phenotypes contribute to kidney injury and repair. *Journal of the American Society of Nephrology : JASN.* 2011;22(2):317-26.
16. Shinoda Y, et al. Tissue transglutaminase exacerbates renal fibrosis via alternative activation of monocyte-derived macrophages. *Cell Death & Disease.* 2023;14(2):136.
17. Murray PJ. Macrophage Polarization. *Annual Review of Physiology.* 2017;79(Volume 79, 2017):541-66.
18. Sibinga NE, et al. Macrophage-restricted and interferon gamma-inducible expression of the allograft inflammatory factor-1 gene requires Pu.1. *The Journal of biological chemistry.* 2002;277(18):16202-10.
19. Yang ZF, et al. Allograft inflammatory factor-1 (AIF-1) is crucial for the survival and pro-inflammatory activity of macrophages. *International immunology.* 2005;17(11):1391-7.

20. Liu G, et al. Allograft inflammatory factor-1 and its immune regulation. *Autoimmunity.* 2007;40(2):95-102.

21. Chinnasamy P, et al. Loss of Allograft Inflammatory Factor-1 Ameliorates Experimental Autoimmune Encephalomyelitis by Limiting Encephalitogenic CD4 T-Cell Expansion. *Molecular medicine (Cambridge, Mass).* 2015;21(1):233-41.

22. Elizondo DM, et al. Allograft inflammatory factor-1 in myeloid cells drives autoimmunity in type 1 diabetes. *JCI insight.* 2020;5(10).

23. Piotrowska K, et al. Over-Expression of Allograft Inflammatory Factor-1 (AIF-1) in Patients with Rheumatoid Arthritis. *Biomolecules.* 2020;10(7).

24. Utans U, et al. Cloning and characterization of allograft inflammatory factor-1: a novel macrophage factor identified in rat cardiac allografts with chronic rejection. *J Clin Invest.* 1995;95(6):2954-62.

25. Nagakawa Y, et al. Over-expression of AIF-1 in liver allografts and peripheral blood correlates with acute rejection after transplantation in rats. *American journal of transplantation : official journal of the American Society of Transplantation and the American Society of Transplant Surgeons.* 2004;4(12):1949-57.

26. Dangi A, et al. Single cell transcriptomics of mouse kidney transplants reveals a myeloid cell pathway for transplant rejection. *JCI insight.* 2020;5(20).

27. Magil AB. Monocytes/macrophages in renal allograft rejection. *Transplant Rev (Orlando).* 2009;23(4):199-208.

28. Mannon RB. Macrophages: contributors to allograft dysfunction, repair, or innocent bystanders? *Curr Opin Organ Transplant.* 2012;17(1):20-5.

29. Le Clef N, et al. Unilateral Renal Ischemia-Reperfusion as a Robust Model for Acute to Chronic Kidney Injury in Mice. *PLoS One.* 2016;11(3):e0152153.

30. Kuivaniemi H, and Tromp G. Type III collagen (COL3A1): Gene and protein structure, tissue distribution, and associated diseases. *Gene.* 2019;707:151-71.

31. Eisner C, et al. Major contribution of tubular secretion to creatinine clearance in mice. *Kidney Int.* 2010;77(6):519-26.

32. Day YJ, et al. Renal ischemia-reperfusion injury and adenosine 2A receptor-mediated tissue protection: role of macrophages. *Am J Physiol Renal Physiol.* 2005;288(4):F722-31.

33. Stein M, et al. Interleukin 4 potently enhances murine macrophage mannose receptor activity: a marker of alternative immunologic macrophage activation. *J Exp Med.* 1992;176(1):287-92.

34. Rőszer T. Understanding the Mysterious M2 Macrophage through Activation Markers and Effector Mechanisms. *Mediators Inflamm.* 2015;2015:816460.

35. Orecchioni M, et al. Macrophage Polarization: Different Gene Signatures in M1(LPS+) vs. Classically and M2(LPS-) vs. Alternatively Activated Macrophages. *Front Immunol.* 2019;10:1084.

36. Apostolopoulos V, and McKenzie IF. Role of the mannose receptor in the immune response. *Curr Mol Med.* 2001;1(4):469-74.

37. Shin NS, et al. Arginase-1 Is Required for Macrophage-Mediated Renal Tubule Regeneration. *Journal of the American Society of Nephrology : JASN.* 2022;33(6):1077-86.

38. Kang Q, et al. An update on Ym1 and its immunoregulatory role in diseases. *Front Immunol.* 2022;13:891220.

39. Meng XM, et al. Macrophage Phenotype in Kidney Injury and Repair. *Kidney Dis (Basel).* 2015;1(2):138-46.

40. Liu J, et al. Wnt/β-catenin signalling: function, biological mechanisms, and therapeutic opportunities. *Signal Transduct Target Ther.* 2022;7(1):3.

41. Tan RJ, et al. Wnt/β-catenin signaling and kidney fibrosis. *Kidney Int Suppl (2011).* 2014;4(1):84-90.

42. Feng Y, et al. Wnt/β-Catenin-Promoted Macrophage Alternative Activation Contributes to Kidney Fibrosis. *Journal of the American Society of Nephrology : JASN.* 2018;29(1):182-93.

43. Xiao L, et al. Sustained Activation of Wnt/β-Catenin Signaling Drives AKI to CKD Progression. *Journal of the American Society of Nephrology.* 2016;27(6).

44. Satoh M, et al. Klotho protects against mouse renal fibrosis by inhibiting Wnt signaling. *American Journal of Physiology-Renal Physiology.* 2012;303(12):F1641-F51.

45. Xu Q, et al. Vascular development in the retina and inner ear: control by Norrin and Frizzled-4, a high-affinity ligand-receptor pair. *Cell.* 2004;116(6):883-95.

46. Casagolda D, et al. A p120-catenin-CK1epsilon complex regulates Wnt signaling. *J Cell Sci.* 2010;123(Pt 15):2621-31.

47. Van den Bossche J, et al. Regulation and function of the E-cadherin/catenin complex in cells of the monocyte-macrophage lineage and DCs. *Blood.* 2012;119(7):1623-33.

48. Gan XQ, et al. Nuclear Dvl, c-Jun, beta-catenin, and TCF form a complex leading to stabilization of beta-catenin-TCF interaction. *J Cell Biol.* 2008;180(6):1087-100.

49. Sato A, et al. WNK regulates Wnt signalling and β-Catenin levels by interfering with the interaction between β-Catenin and GID. *Communications Biology.* 2020;3(1):666.

50. Golan T, et al. The human Frizzled 6 (HFz6) acts as a negative regulator of the canonical Wnt. beta-catenin signaling cascade. *The Journal of biological chemistry.* 2004;279(15):14879-88.

51. Kawano Y, and Kypta R. Secreted antagonists of the Wnt signalling pathway. *J Cell Sci.* 2003;116(Pt 13):2627-34.

52. Relloso M, et al. DC-SIGN (CD209) expression is IL-4 dependent and is negatively regulated by IFN, TGF-beta, and anti-inflammatory agents. *J Immunol.* 2002;168(6):2634-43.

53. Loke P, et al. IL-4 dependent alternatively-activated macrophages have a distinctive in vivo gene expression phenotype. *BMC Immunol.* 2002;3:7.

54. Wong KL, et al. Gene expression profiling reveals the defining features of the classical, intermediate, and nonclassical human monocyte subsets. *Blood.* 2011;118(5):e16-31.

55. Yin C, et al. Efferocytic Defects in Early Atherosclerosis Are Driven by GATA2 Overexpression in Macrophages. *Front Immunol.* 2020;11:594136.

56. Snarski P, et al. Macrophage-Specific IGF-1 Overexpression Reduces CXCL12 Chemokine Levels and Suppresses Atherosclerotic Burden in Apoe-Deficient Mice. *Arterioscler Thromb Vasc Biol.* 2022;42(2):113-26.

57. Lee S, et al. Arf6 exacerbates allergic asthma through cell-to-cell transmission of ASC inflammasomes. *JCI insight.* 2021;6(16).

58. Zhang L, et al. Peli1 facilitates NLRP3 inflammasome activation by mediating ASC ubiquitination. *Cell Rep.* 2021;37(4):109904.

59. Langlais D, et al. The macrophage IRF8/IRF1 regulome is required for protection against infections and is associated with chronic inflammation. *J Exp Med.* 2016;213(4):585-603.

60. Jiang Z, et al. Calreticulin Blockade Attenuates Murine Acute Lung Injury by Inducing Polarization of M2 Subtype Macrophages. *Front Immunol.* 2020;11:11.

61. Pawar NM, and Rao P. Secreted frizzled related protein 4 (sFRP4) update: A brief review. *Cellular Signalling.* 2018;45:63-70.

62. Hou J, et al. M2 macrophages promote myofibroblast differentiation of LR-MSCs and are associated with pulmonary fibrogenesis. *Cell Commun Signal.* 2018;16(1):89.

63. Lake BB, et al. An atlas of healthy and injured cell states and niches in the human kidney. *Nature.* 2023;619(7970):585-94.

64. Wilson PC, et al. Multimodal single cell sequencing implicates chromatin accessibility and genetic background in diabetic kidney disease progression. *Nat Commun.* 2022;13(1):5253.

65. Hinze C, et al. Single-cell transcriptomics reveals common epithelial response patterns in human acute kidney injury. *Genome Med.* 2022;14(1):103.

66. Li L, et al. NKT cell activation mediates neutrophil IFN-gamma production and renal ischemia-reperfusion injury. *J Immunol.* 2007;178(9):5899-911.

67. Ascon DB, et al. Phenotypic and functional characterization of kidney-infiltrating lymphocytes in renal ischemia reperfusion injury. *J Immunol.* 2006;177(5):3380-7.

68. Dai H, et al. Donor SIRPα polymorphism modulates the innate immune response to allogeneic grafts. *Science Immunology.* 2017;2(12):eaam6202.

69. Oberbarnscheidt MH, et al. Non-self recognition by monocytes initiates allograft rejection. *The Journal of Clinical Investigation.* 2014;124(8):3579-89.

70. Guiteras R, et al. Macrophage in chronic kidney disease. *Clin Kidney J.* 2016;9(6):765-71.

71. Dong Y, et al. Ischemic Duration and Frequency Determines AKI-to-CKD Progression Monitored by Dynamic Changes of Tubular Biomarkers in IRI Mice. *Front Physiol.* 2019;10:153.

72. Sato Y, and Yanagita M. Immune cells and inflammation in AKI to CKD progression. *Am J Physiol Renal Physiol.* 2018;315(6):F1501-f12.

73. Yang Z, and Ming XF. Functions of arginase isoforms in macrophage inflammatory responses: impact on cardiovascular diseases and metabolic disorders. *Front Immunol.* 2014;5:533.

74. Shosha E, et al. The arginase 1/ornithine decarboxylase pathway suppresses HDAC3 to ameliorate the myeloid cell inflammatory response: implications for retinal ischemic injury. *Cell Death & Disease.* 2023;14(9):621.

75. Fouda AY, et al. Targeting proliferative retinopathy: Arginase 1 limits vitreoretinal neovascularization and promotes angiogenic repair. *Cell Death & Disease.* 2022;13(8):745.

76. Miller-Fleming L, et al. Remaining Mysteries of Molecular Biology: The Role of Polyamines in the Cell. *J Mol Biol.* 2015;427(21):3389-406.

77. He W, et al. Wnt/β-catenin signaling promotes renal interstitial fibrosis. *Journal of the American Society of Nephrology.* 2009;20(4):765-76.

78. Palevski D, et al. Loss of Macrophage Wnt Secretion Improves Remodeling and Function After Myocardial Infarction in Mice. *Journal of the American Heart Association.* 2017;6(1):e004387.

79. Tsubata Y, et al. Expression of allograft inflammatory factor-1 in kidneys: A novel molecular component of podocyte. *Kidney Int.* 2006;70(11):1948-54.

80. Autieri MV, et al. Expression of allograft inflammatory factor-1 is a marker of activated human vascular smooth muscle cells and arterial injury. *Arterioscler Thromb Vasc Biol.* 2000;20(7):1737-44.

81. Tian Y, et al. AIF-1 expression regulates endothelial cell activation, signal transduction, and vasculogenesis. *Am J Physiol Cell Physiol.* 2009;296(2):C256-66.

82. Scarfe L, et al. Long-term outcomes in mouse models of ischemia-reperfusion-induced acute kidney injury. *Am J Physiol Renal Physiol.* 2019;317(4):F1068-f80.

83. Casimiro I, et al. Genetic inactivation of the allograft inflammatory factor-1 locus. *Genesis.* 2013;51(10):734-40.

84. Van Gassen S, et al. FlowSOM: Using self-organizing maps for visualization and interpretation of cytometry data. *Cytometry Part A.* 2015;87(7):636-45.

85. Ide S, et al. Ferroptotic stress promotes the accumulation of pro-inflammatory proximal tubular cells in maladaptive renal repair. *Elife.* 2021;10.

86. Ide S, et al. Sex differences in resilience to ferroptosis underlie sexual dimorphism in kidney injury and repair. *Cell Rep.* 2022;41(6):111610.

87. Hao Y, et al. Integrated analysis of multimodal single-cell data. *Cell.* 2021;184(13):3573-87.e29.

88. McGinnis CS, et al. DoubletFinder: Doublet Detection in Single-Cell RNA Sequencing Data Using Artificial Nearest Neighbors. *Cell Syst.* 2019;8(4):329-37.e4.

89. Korsunsky I, et al. Fast, sensitive and accurate integration of single-cell data with Harmony. *Nat Methods.* 2019;16(12):1289-96.

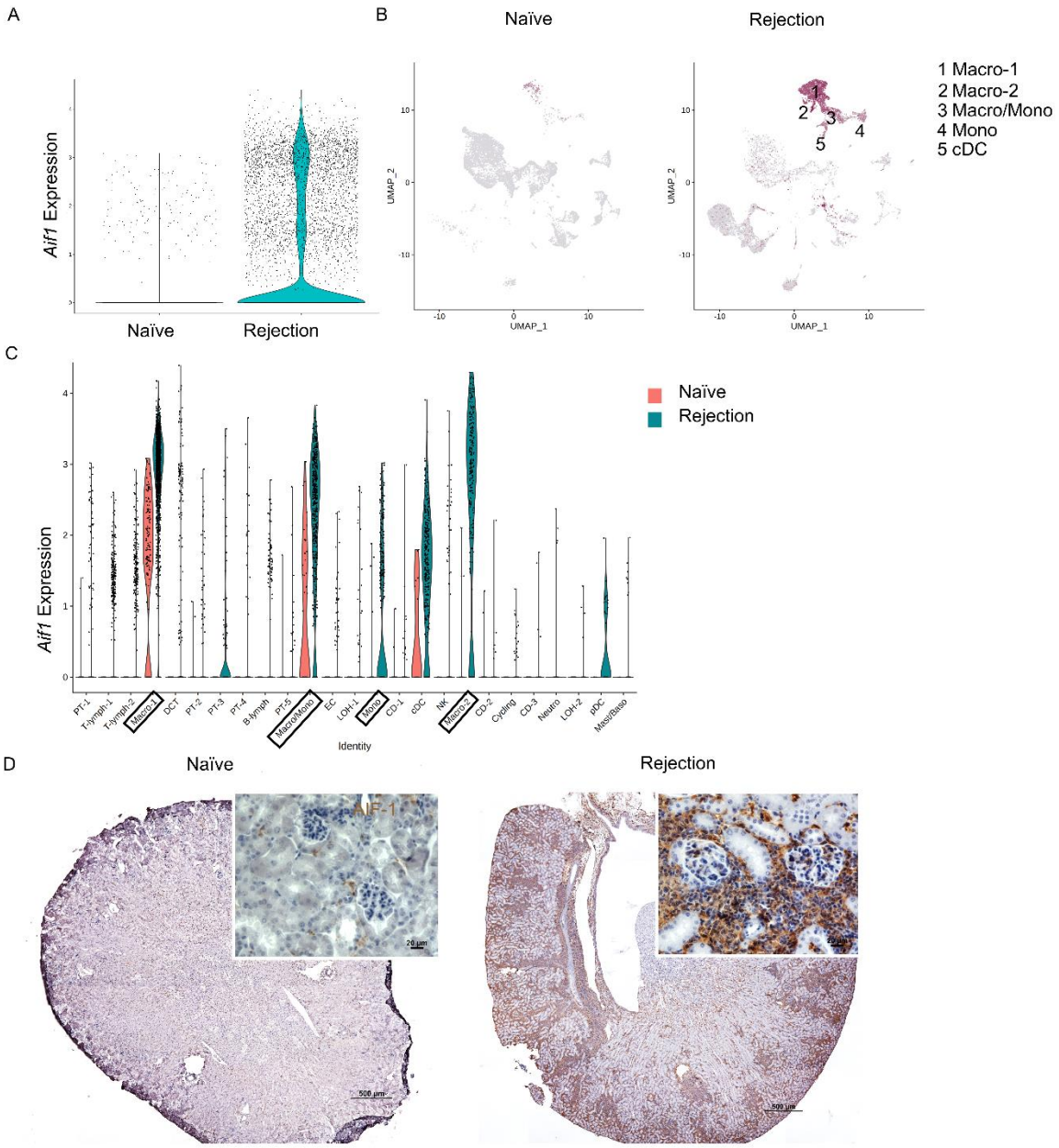

Figure 1. Kidney macrophages upregulate AIF-1 following kidney injury. (A-C) Single cell sequencing analysis of Allograft inflammatory factor-1 (*Aif1*) expressing cells in murine allogeneic kidney transplantation. Day15 post-transplant (BALB/c kidneys transplanted into bilateral nephrectomised B6 recipients) and naïve unmanipulated BALB/c kidneys were used as controls (n=2 each). (A) Violin plot showing total *Aif1* expression levels in naïve and rejection kidneys. (B) Feature plots for naïve and rejecting kidneys showing that myeloid cell subsets were the

predominant cell populations expressing *Aif1*. (C) Violin plots showing *Aif1* expression level by cell type in both naïve and rejection samples. (D) Immunohistochemical staining for AIF-1 (brown) in naïve kidneys and rejecting kidneys at Day15 post-transplant. Images are representative of n=3 each. 100x magnification for stitch images, insets: 400x magnification. Scale bars 500µm and 20µm respectively. PT, proximal tubule; T-lymph, T lymphocyte; Macro, macrophage; DCT, distal convoluted tubule; B-lymph, B lymphocyte; Macro/Mono, macrophage/monocyte; EC, endothelial cell; LOH, Loop of Henle; CD, collecting duct; cDC, conventional DC; Neutro, neutrophil; pDC, plasmacytoid DC; Mast/Baso, mast cell/basophil.

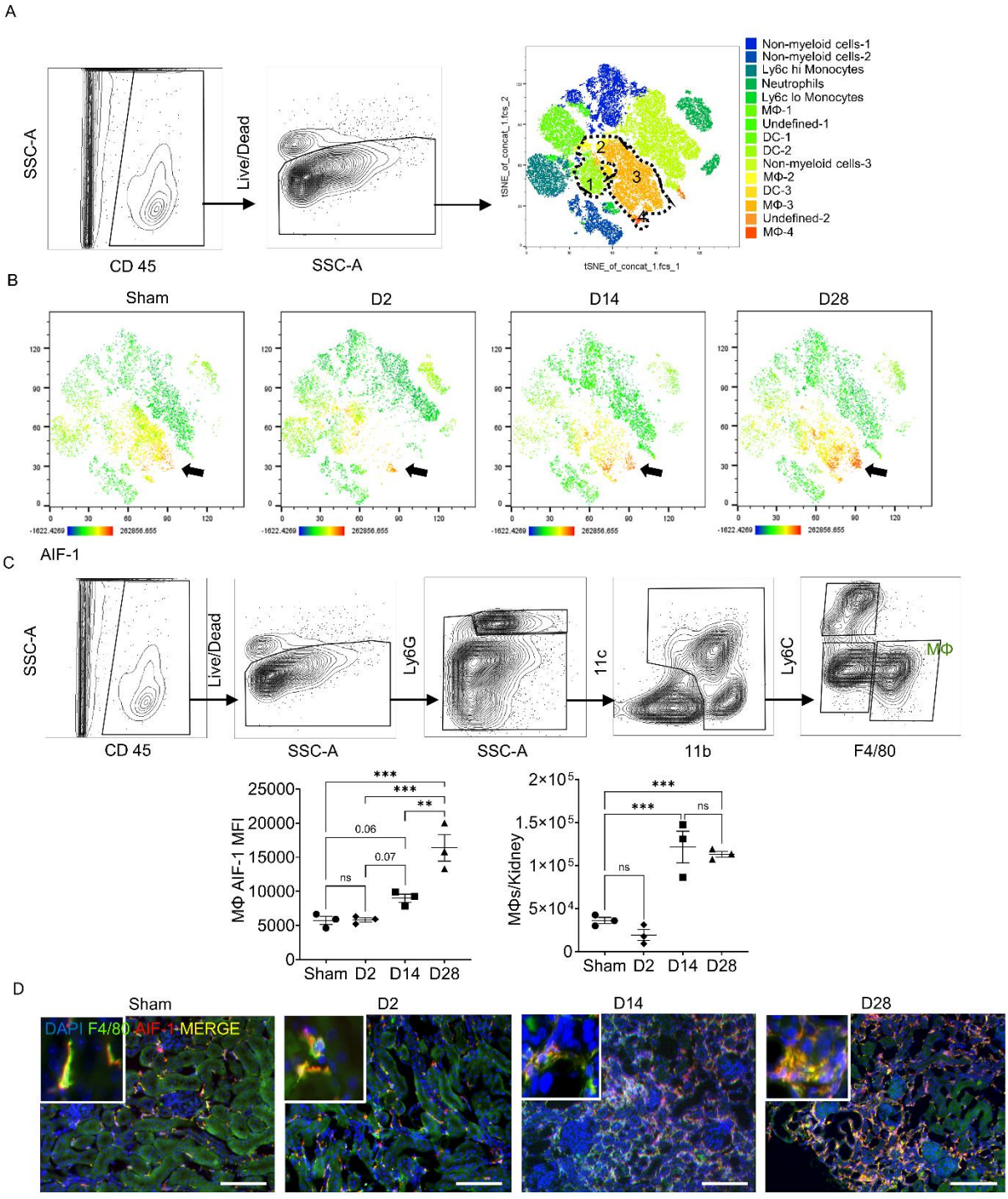

Figure 2. Kinetics of AIF-1 expression and macrophage (MΦ) infiltration in the kidney after ischemia reperfusion injury (I/RI). B6 mice underwent unilateral left kidney I/RI or sham surgery and kidneys were collected at day2, day14 and day28 post I/RI. Flow cytometry-based cell type annotation and AIF-1 expression are shown in (A-C). For (A-C), n=3 for each group. (A) Gating

strategy and tSNE plot gated on $CD45^+$ live cells from all groups and all time points, showing 14 immune cell clusters; cell clusters encircled with the dotted line were annotated as MΦs (MΦ 1-4). (B) tSNE plots separated by sham-operated, day2, day14 and day28 showing AIF-1 expression. (C) Gating strategy for kidney MΦs. Graphs show kidney MΦ AIF-1 MFI and total MΦs per kidney. Each symbol represents data from an individual mouse. Error bars are mean ± SEM. ***P* <0.01, ****P* <0.001, ns: not significant. (D) Immunofluorescence staining of kidney sections for F4/80 and AIF-1. Images are representative of n=3 mice for Sham, n=6 mice for day2 and day14 post I/RI (D2, D14) and n=8 mice for day28 post IRI (D28). Original magnification: x200. Scale bar = 100μm. MΦ, Macrophage; DC, Dendritic Cell; MFI, Mean Fluorescence Intensity. For (C) statistical analysis was performed using one-way ANOVA with Tukey's multiple-comparison test.

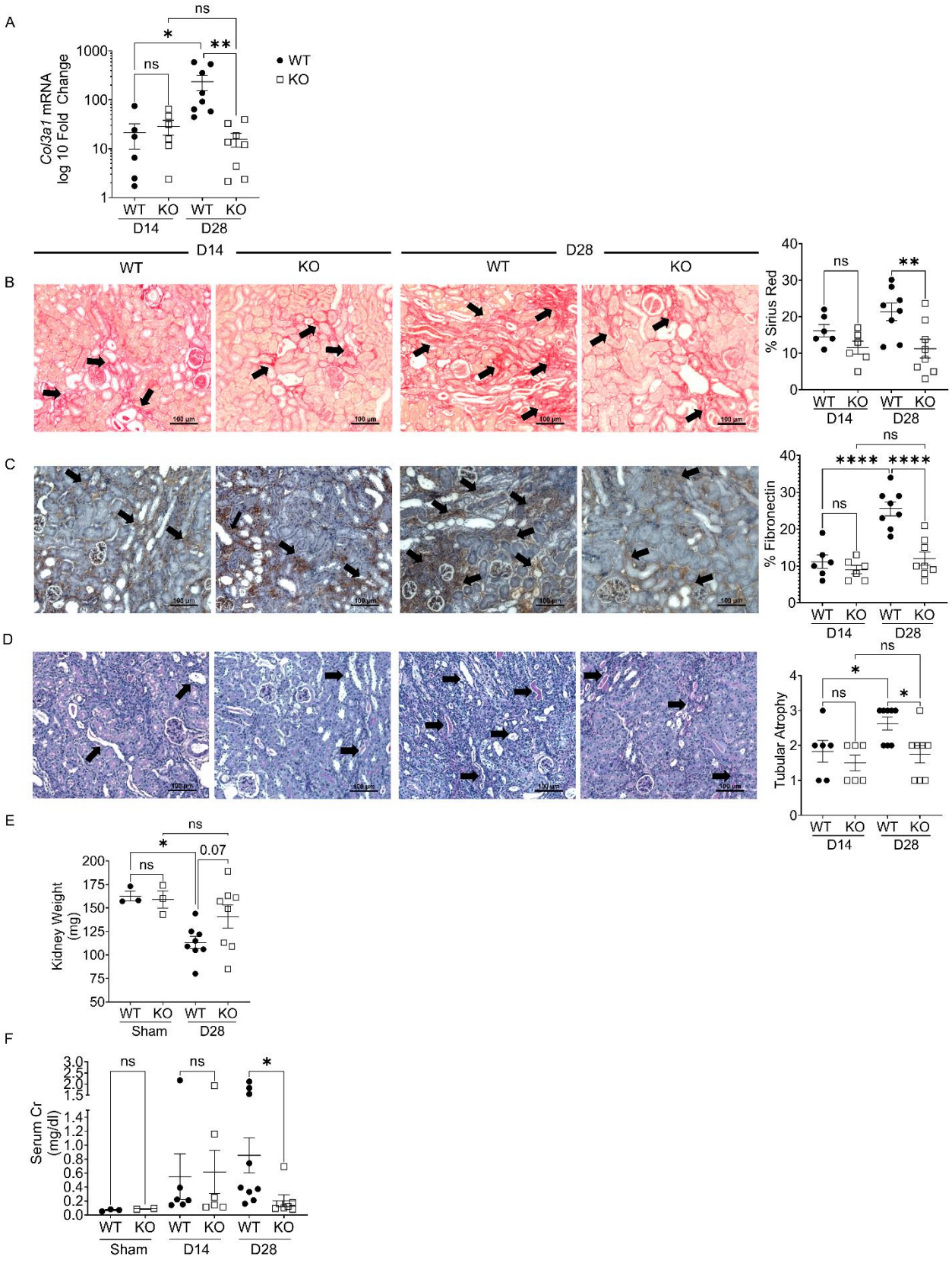
A
Col3a1 mRNA
log 10 Fold Change
1000
100
10
1
ns
*
**
ns
WT
KO
WT KO WT KO
D14 D28
B
D14
D28
WT
KO
WT
KO
% Sirius Red
40
30
20
10
0
ns
**
WT KO WT KO
D14 D28
C
% Fibronectin
40
30
20
10
0
ns
****
****
ns
WT KO WT KO
D14 D28
D
Tubular Atrophy
4
3
2
1
0
ns
*
ns
*
WT KO WT KO
D14 D28
E
Kidney Weight
(mg)
200
175
150
125
100
75
50
ns
*
0.07
ns
WT KO WT KO
Sham D28
F
Serum Cr
(mg/dl)
3.0
2.5
2.0
1.5
1.4
1.2
1.0
0.8
0.6
0.4
0.2
0.0
ns
ns
*
WT KO WT KO WT KO
Sham D14 D28

Figure 3. *Aif1* knockout (KO) attenuates kidney fibrosis and atrophy. (A) Collagen type III alpha chain 1 (*Col3a1*) mRNA in the indicated groups was measured by reverse transcription quantitative polymerase chain reaction (RT-qPCR). Data is presented on a Log10 axis. (B) Images and quantification graph of Sirius Red staining of the kidney in indicated groups. (C) Images and quantification graph of fibronectin staining of the kidney in indicated groups. (D) Images of hematoxylin and eosin staining of kidney sections and quantification graph of tubular atrophy in the indicated groups. (E) Kidney weights in milligrams (mg) of the indicated groups. (F) Kidney function by serum creatinine (Cr) of the indicated groups. For (A-F), each symbol represents data from an individual mouse. For (B-D), images are representative of n=6 each for WT and KO for day 14 post I/RI (D14) and n=8 each for WT and KO for day 28 post I/RI (D28). Original magnification: x200. Scale bar = 100 μm. Black arrows denote positive areas. Error bars are mean ± SEM. **P* <0.05, ***P* <0.01, *****P*<0.0001, ns: not significant. WT, wild-type; KO, *Aif1* knock-out; mg, milligrams, Cr, creatinine. For (A-F) statistical analysis was performed using one-way ANOVA with Tukey's multiple-comparison test.

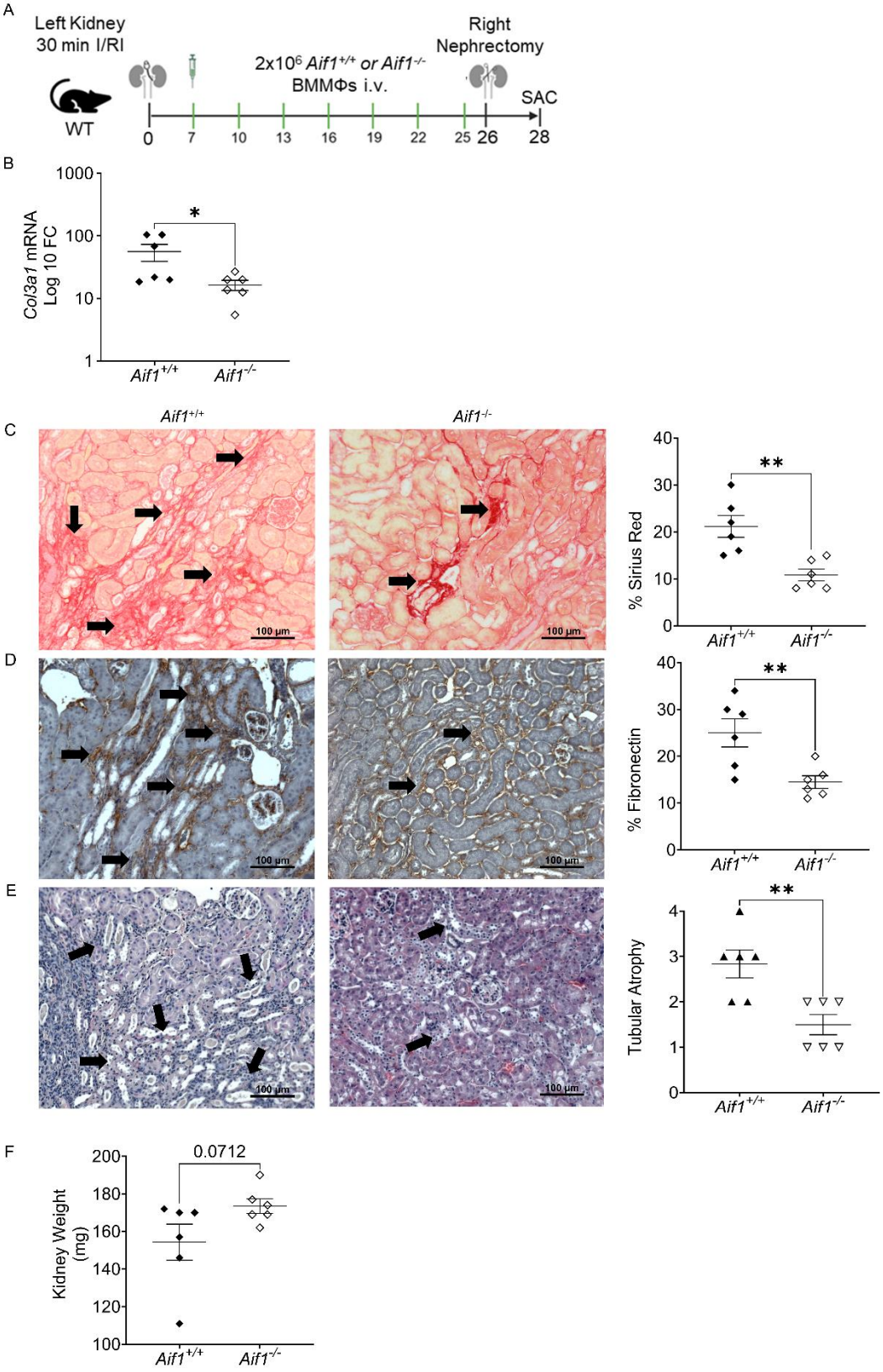
A
Left Kidney
30 min I/RI
WT
2x10⁶ Aif1+/+ or Aif1-/-
BMMΦs i.v.
Right
Nephrectomy
SAC
0 7 10 13 16 19 22 25 26 28
B
Col3a1 mRNA
Log 10 FC
1000
100
10
1
*
Aif1+/+
Aif1-/-
C
Aif1+/+
Aif1-/-
100 µm
% Sirius Red
40
30
20
10
0
**
D
% Fibronectin
E
Tubular Atrophy
4
3
2
1
0
F
Kidney Weight
(mg)
200
180
160
140
120
100
0.0712

Figure 4. Adoptive Transfer of *Aif1*$^{-/-}$ macrophages alleviates fibrosis following I/RI in WT mice. (A) Schema of the model for I/RI and adoptive transfer of *Aif1*$^{+/+}$ and *Aif1*$^{-/-}$ bone marrow derived macrophages (BMMΦs). (B) Collagen type III alpha chain 1 (*Col3a1*) mRNA in the indicated groups was measured by RT-qPCR. Data is presented on a Log10 axis. (C) Images and quantification graph of Sirius Red staining of the kidney in indicated groups. (D) Images and quantification graph of fibronectin staining of the kidney in indicated groups. (E) Images of hematoxylin and eosin staining of kidney sections and quantification graph of tubular atrophy in the indicated groups. (F) Kidney weights in milligrams (mg) of the indicated groups. For (B-F) each symbol represents data from an individual mouse. For (C-E), images are representative of n=6 per group. Black arrows denote positive areas. Original magnification: x200. Scale bar = 100 μm. Error bars are mean ± SEM. **P* <0.05, ***P* <0.01, ****P* <0.001 ns: not significant. BMMΦ, bone marrow macrophage; i.v, intravenous; I/RI, ischemic reperfusion injury; Sac, sacrifice; mg, milligrams. For (B-F) statistical analysis was performed using unpaired 2 tailed student's *t* test.

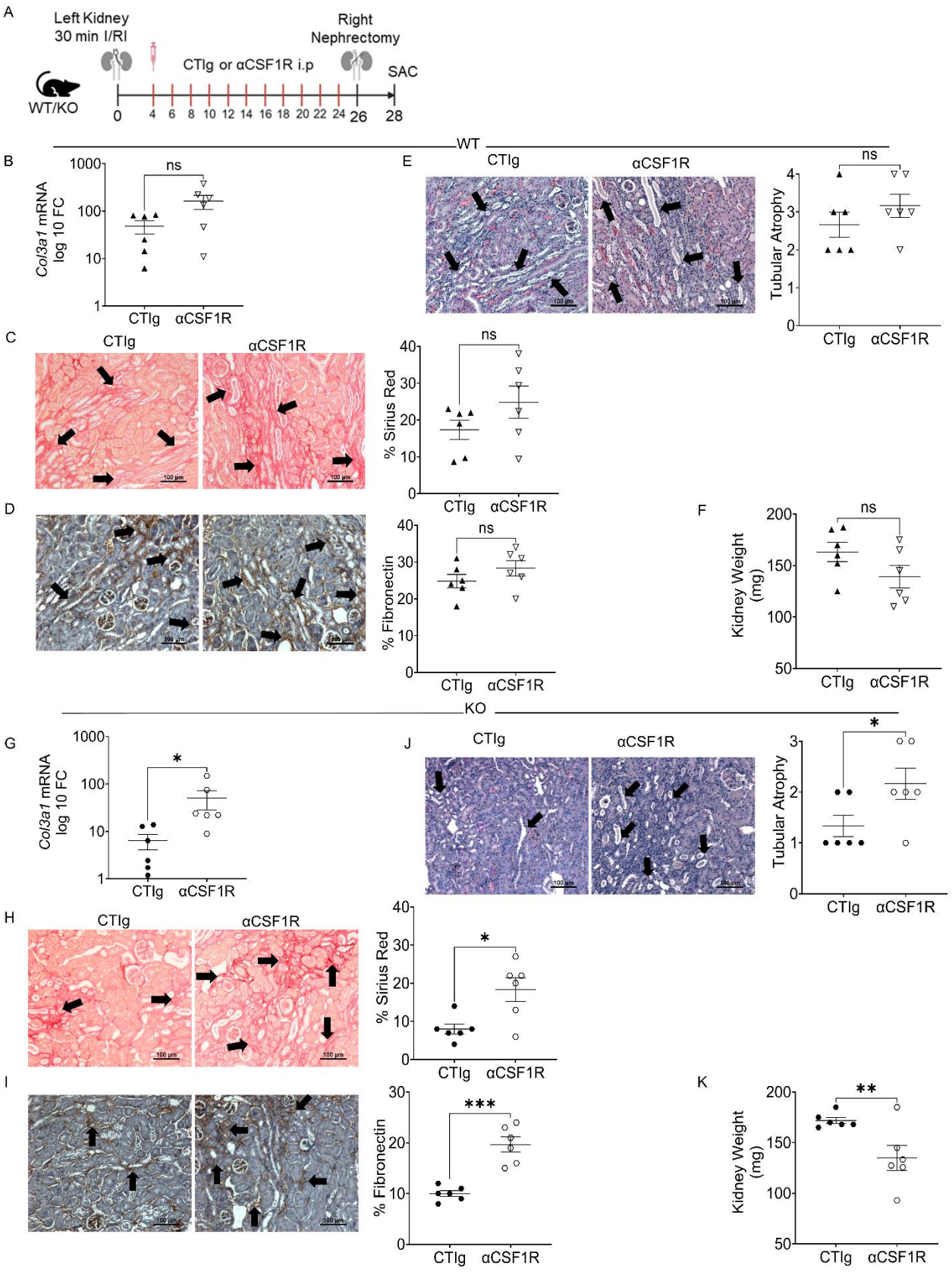
A
Left Kidney
30 min I/RI
Right
Nephrectomy
CTlg or αCSF1R i.p
SAC
WT/KO
0 4 6 8 10 12 14 16 18 20 22 24 26 28
WT
B
Col3a1 mRNA
log 10 FC
ns
CTlg αCSF1R
C
CTlg
αCSF1R
% Sirius Red
ns
D
% Fibronectin
ns
E
CTlg
αCSF1R
Tubular Atrophy
ns
F
Kidney Weight
(mg)
ns
KO
G
Col3a1 mRNA
log 10 FC
*
H
% Sirius Red
*
I
% Fibronectin
***
J
Tubular Atrophy
*
K
Kidney Weight
(mg)
**

Figure 5. Macrophage depletion in *Aif1* KO mice worsens fibrosis and atrophy after I/RI. (A) Schema of the model for I/RI and administration of anti-colony stimulating factor-1 receptor antibody (αCSF1R) or control immunoglobulin (CTIg). (B-F): data from WT mice. (B) Collagen type III alpha chain 1 (*Col3a1*) mRNA in WT mice treated with CTIg and αCSF1R was measured by RT-qPCR. Data is presented on a Log10 axis. (C) Images and quantification graph of Sirius Red staining of the kidney in indicated groups. (D) Images and quantification graph of fibronectin staining of the kidney in indicated groups. (E) Images of hematoxylin and eosin staining of kidney sections and quantification graph of tubular atrophy in the indicated groups. (F) Kidney weights in milligrams (mg) of the indicated groups. (G-K): same as (B-F) except in KO mice. For (B-K), each symbol represents data from an individual mouse. For (C-E, H-J), images are representative of n=6 for each group. Error bars are mean ± SEM. **P* <0.05, ***P* <0.01, ****P*<0.001 ns: not significant. WT, wild-type; KO, *Aif1* knock-out; BMMΦ, bone marrow macrophage; i.p, intraperitoneal; I/RI, ischemic reperfusion injury; Sac, sacrifice; mg, milligrams. For (B-K) statistical analysis was performed using unpaired 2 tailed student's *t* test.

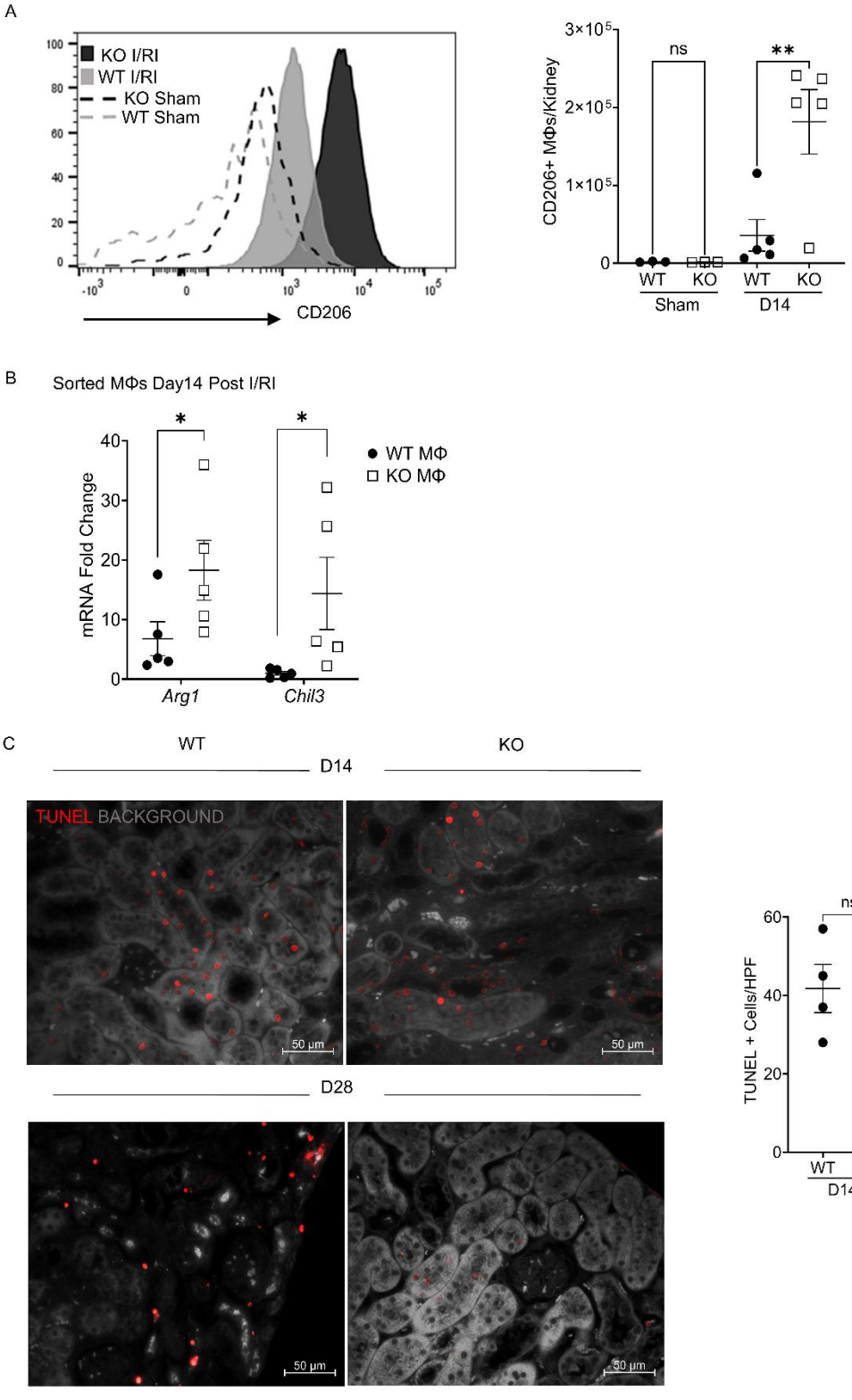
A
KO I/RI
WT I/RI
KO Sham
WT Sham
CD206
CD206+ MΦs/Kidney
ns
**
WT
KO
WT
KO
Sham
D14
B
Sorted MΦs Day14 Post I/RI
mRNA Fold Change
WT MΦ
KO MΦ
*
*
Arg1
Chil3
C
WT
KO
D14
D28
TUNEL BACKGROUND
50 µm
TUNEL + Cells/HPF
ns
*
WT
KO
WT
KO
D14
D28

Figure 6. *Aif1* deletion enhances macrophage reparative functions. (A) Representative histogram and quantification graph showing $CD206^+$ macrophages (MΦ) in the kidney at day14 (D14) post I/RI or sham surgery in WT and KO mice. (B) Kidney macrophages were immunomagnetically purified on day14 post I/RI or sham surgery and gene expression using RT-qPCR was quantified for arginase1 (*Arg1*) and chitinase-like 3 (*Chil3*). Expression was normalized to sorted macrophages from sham-operated mice. (C) Representative images of TUNEL staining of kidney sections and quantification graph of the indicated groups. Images are representative of n=4 each for D14 and D28 post I/RI. Original magnification: x200. Scale bar = 50 µm. For (A-C) each symbol represents data from an individual mouse. Error bars are mean ± SEM. **P* <0.05, ***P* <0.01, ns: not significant. WT, wild-type; KO, *Aif1* knockout; HPF, high power field (200x). For (A-C) statistical analysis was performed using one-way ANOVA with Tukey's multiple-comparison test.

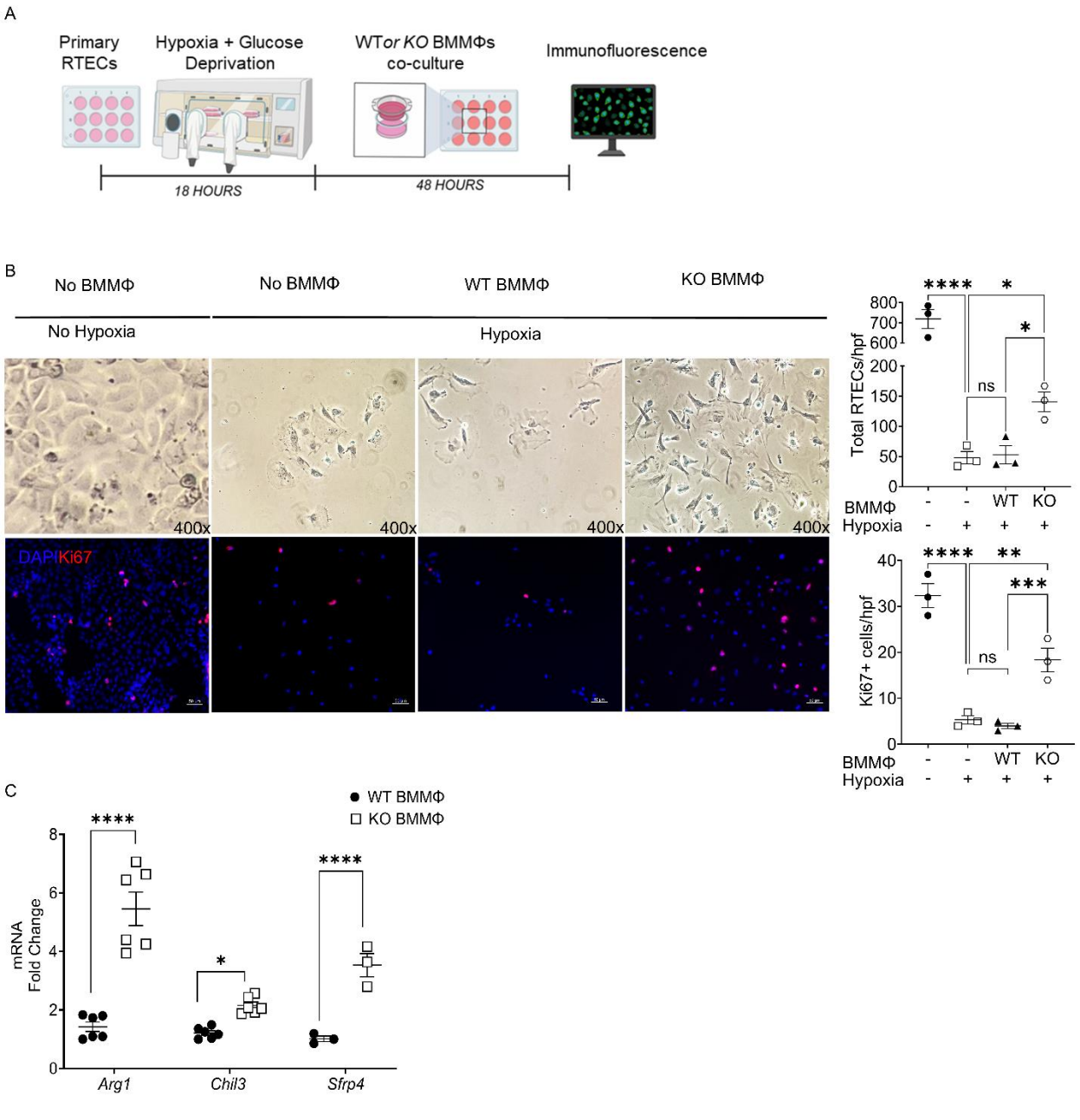

Figure 7. *Aif1*$^{-/-}$ macrophages protect renal tubular epithelial cells (RTEC) from hypoxic injury *in vitro*. (A) Model of RTECs hypoxia and reoxygenation followed by transwell co-culture with bone marrow macrophages (BMMΦs) from *Aif1* KO and WT mice. (B) Upper panels: representative brightfield microscopy images of RTECs from the indicated groups. Magnification= 400x. Lower panels: representative immunofluorescent image with DAPI (blue) and Ki67(red)

staining of RTECs from the same groups. Magnification = 200x. Scale bars = 50 μm. Images are representative of n=3 for each group. Quantification graphs show (1) Total RTECs/hpf ($DAPI^+$ cells) and (2) $Ki67^+$ cells/hpf. (C) WT and KO BMMΦs were treated with conditioned media (CM) from RTECs subjected to 18-hour hypoxia followed by 48-hour re-oxygenation. BMMΦs were cultured in the CM for a total of 48 hours, and harvested for RT-qPCR. Expression of arginase-1 (*Arg1*), chitinase-like 3 (*Chil3*), secreted frizzled protein 4 (*Sfrp4*) are shown. Data was normalized to expressions in WT BMMΦs. For (B, C), each symbol represents data from an individual mouse . Error bars are mean ± SEM. **P* <0.05, ***P* <0.01, ****P*<0.001, *****P*<0.0001; ns: not significant. Experiments were repeated twice. hpf, high power field, WT, wild-type; KO, *Aif1* knock-out. For (B-C) statistical analysis was performed using one-way ANOVA with Tukey's multiple-comparison test.

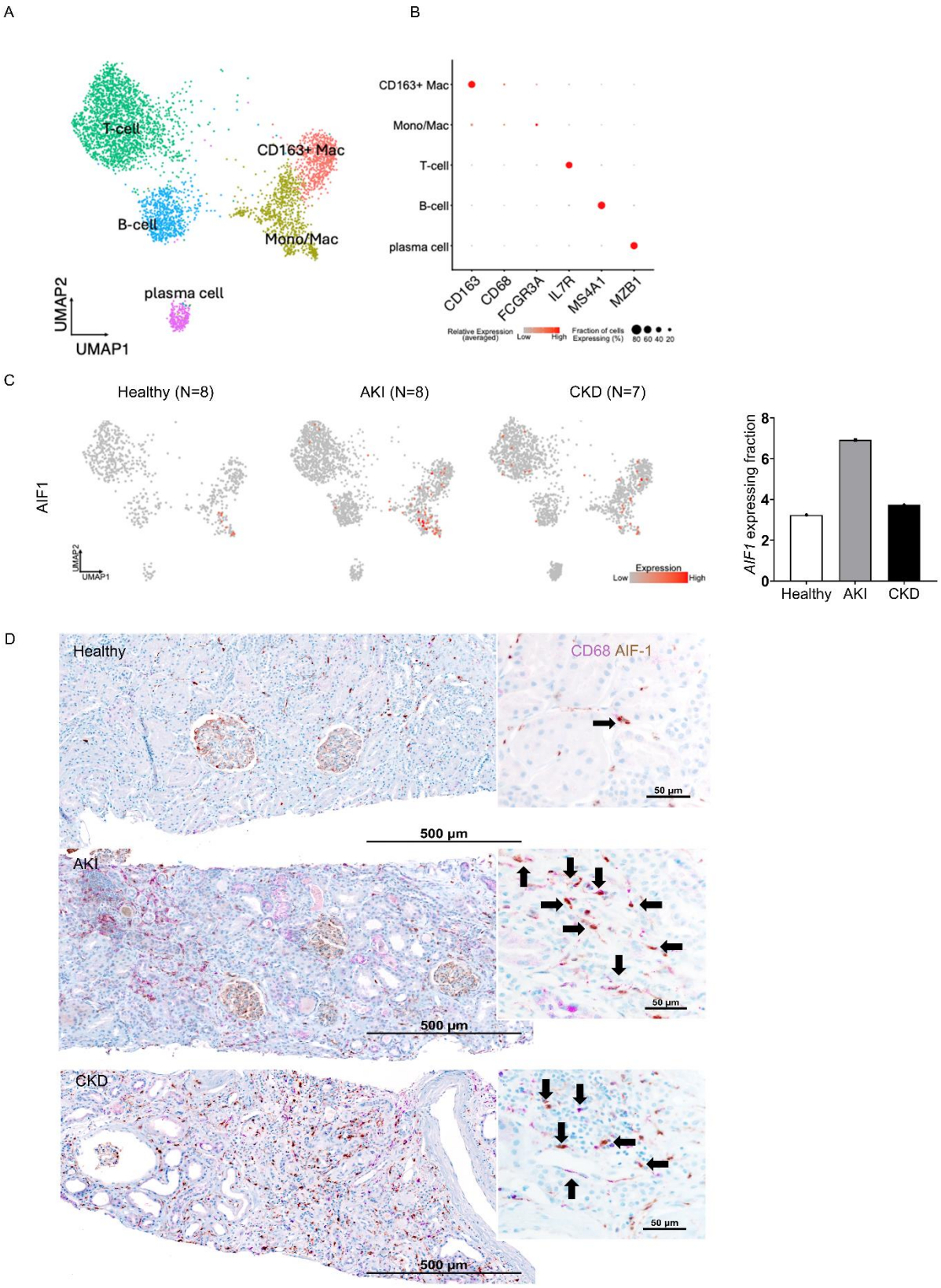
A
T-cell
CD163+ Mac
B-cell
Mono/Mac
plasma cell
UMAP2
UMAP1
B
CD163+ Mac
Mono/Mac
T-cell
B-cell
plasma cell
CD163
CD68
FCGR3A
IL7R
MS4A1
MZB1
Relative Expression (averaged)
Low
High
Fraction of cells Expressing (%)
80 60 40 20
C
Healthy (N=8)
AKI (N=8)
CKD (N=7)
AIF1
UMAP2
UMAP1
Expression
Low
High
AIF1 expressing fraction
8
6
4
2
0
Healthy
AKI
CKD
D
Healthy
CD68 AIF-1
50 μm
500 μm
AKI
50 μm
500 μm
CKD
50 μm
500 μm

Figure 8. *Aif-1* is expressed in human kidneys with AKI or CKD. (A-C) Single nuclear sequencing of kidney biopsy samples from healthy individuals (n=8), patients with acute kidney injury (AKI) (n=8), or chronic kidney disease (CKD) (n=7). (A) A composite Uniform Manifold Approximation and Projection (UMAP) plot of all samples (total n=23) showing 5 unique immune cell clusters. (B) Dot plot showing canonical marker expressions used for cell type annotation. (C) Individual feature plots separated by disease states (as indicated) showing *AIF1* expression. *AIF1* expression is more pronounced in AKI and CKD compared to healthy controls within the monocyte/macrophage (Mono/Mac) and the CD163+ macrophage (CD163+ Mac) subsets. Quantification graph shows the percentage of *Aif1*-expressing cells among total (Mono/Mac and CD163+ Mac) cells by disease state. (D) Immunohistochemical staining for CD68 (purple) and AIF-1(brown) in human biopsy samples of native kidneys (n=3 each for healthy, AKI and CKD). 200x magnification for stitch images, inset: 400x magnification. Scale bars: 500µm and 50µm respectively. T-cell, T lymphocyte; B-cell, B lymphocyte; Mac, macrophage; Mono, monocyte. For (A-C), results are based on data collected by the Kidney Precision Medicine Project. Accessed March 11, 2023. https://www.kpmp.org.